JOURNAL OF SPACECRAFT AND ROCKETS
Vol. 32, No. 1, January–February 1995

Review and Development of Base Pressure and Base Heating Correlations in Supersonic Flow

J. Parker Lamb
University of Texas at Austin, Austin, Texas 78712
and
William L. Oberkampf
Sandia National Laboratories, Albuquerque, New Mexico 87185

A comprehensive review of experimental base pressure and base heating data related to supersonic and hypersonic flight vehicles is presented. Particular attention is paid to free-flight data as well as wind-tunnel data for models without rear sting support. Using theoretically based correlation parameters, a series of internally consistent, empirical predictions are developed for planar and axisymmetric geometries (wedges, cones, and cylinders). These equations encompass the speed range from low supersonic to hypersonic flow and laminar and turbulent forebody boundary layers. A wide range of cone and wedge angles and cone bluntness ratios is included in the data base used to develop the correlations. The present investigation also includes an analysis of the effect of the angle of attack and the specific-heat ratio of the gas. Angle-of-attack effects are considered on sharp and blunted cones and cylindrical afterbodies.

Nomenclature

C = Crocco number
C_D = drag coefficient
C_p = pressure coefficient
D = base diameter
H = total (stagnation) enthalpy
$\boldsymbol{H}$ = base height or base radius
h = static enthalpy
L = body length
M = Mach number
P = pressure
$\dot{q}$ = convective heat transfer rate per unit area
R = Reynolds number
R' = unit Reynolds number
r_b = body or base radius
r_n = nose radius
St = Stanton number
s = body surface length
T = temperature
u = velocity
x = longitudinal coordinate
y = transverse coordinate
α = angle of attack
γ = ratio of specific heats
δ = boundary-layer thickness
η = transverse coordinate in Lees-Dorodnitsyn transformation
θ = boundary-layer momentum thickness
θ_c = cone half angle
ν = Prandtl-Meyer angle

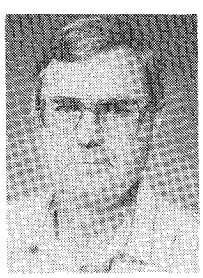

William L. Oberkampf is a Senior Member of Technical Staff in the Aerosciences and Fluid Dynamics Department at Sandia National Laboratories, Albuquerque, New Mexico. After completing his Ph.D., he joined the faculty of the Mechanical Engineering Department at the University of Texas at Austin. In 1979 he joined Sandia and has worked in both staff and management positions in research and development. During his professional career he has worked in the areas of computational fluid dynamics, high angle of attack aerodynamics, hypersonics, experimental aerodynamics and wind tunnel testing, hydrodynamics, and cavitating flow, and recently in thermal spray coating technology. The author received his B.S. in Aerospace Engineering from the University of Notre Dame (1966), his M.S. in Mechanical Engineering from the University of Texas at Austin (1967), and his Ph.D. in Aerospace Engineering from the University of Notre Dame (1970). He is an Associate Fellow of the AIAA.

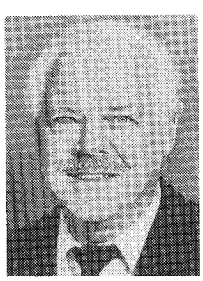

J. Parker Lamb is Ernest Cockrell Jr. Memorial Professor in the Department of Mechanical Engineering at The University of Texas at Austin. A member of the UT Austin faculty since 1963, he has served as Chairman of the Department of Mechanical Engineering, Associate Dean of Engineering, and Chairman of the Department of Aerospace Engineering and Engineering Mechanics. He has made numerous research contributions to the area of fluid flow and convective heat transfer in recirculating flow fields, ranging from low speed flow past surfaces with discrete roughness to hypersonic flows of tandem projectiles. During his academic career he has been associated, as consultant or temporary employee, with a number of aerospace organizations including Arnold Engineering Development Center, LTV Aerospace, NASA Marshall Space Flight Center, and Sandia National Laboratories. The author received a B.S. in Mechanical Engineering from Auburn University (1954) and a Ph.D. in Mechanical Engineering from the University of Illinois at Urbana-Champaign (1961). He is an Associate Fellow of AIAA.

Received Jan. 31, 1994; revision received Oct. 17, 1994; accepted for publication Oct. 27, 1994.

ξ = longitudinal coordinate in Lees-Dorodnitsyn transformation
ρ = fluid density

Subscripts

a = axial direction
b = base plane
e = edge of boundary layer
ef = effective value
g = arbitrary gas
s = body surface length
w = wall conditions
0 = stagnation conditions
1 = conditions upstream of cylinder shoulder
∞ = freestream condition

Introduction

BASE drag of projectiles is one of the oldest topics of applied aerodynamics. Although it has been studied and analyzed for well over a century, reliable prediction of it is still beyond the reach of modern numerical simulation. The importance of base drag on a slender vehicle in supersonic flight is illustrated in Fig. 1. The relative size of the three components of drag (base, wave, and skin friction) for a slender cone at zero angle of attack are plotted in Fig. 1 against freestream Mach number.[1] Recall that 1) base drag represents the loss in recovery of pressure over the base of the body, 2) wave drag, or forebody pressure drag, is the axial component of the integral of surface pressure over the forebody area, and 3) skin friction drag is the axial component of surface shear stress over the forebody. For slender bodies, even with blunted noses, the skin friction drag and wave drag do not vary substantially with freestream Mach number. However, the base drag decreases in absolute value as the Mach number increases. As the slenderness ratio of the vehicle decreases, the base drag becomes a smaller portion of the total drag, primarily because the wave drag increases significantly. Also, for winged or finned vehicles the proportion of drag due to the base is reduced because of the increased drag on lifting and control surfaces. Regardless of the proportion of base drag to total drag, the computation of trajectories for flight vehicles requires accurate estimates of the base drag component and thus the base pressure.

Although computational techniques have advanced in recent years to a level that includes reasonable prediction of near-wake flow fields in the laminar regime, less accuracy can be obtained for turbulent wakes because of the lack of reliable models for turbulence. Also, near-wake flow computations are complex, extremely computer-intensive, and often expensive. Therefore, we must turn to correlations of test data to obtain estimates of base pressure for most cases of practical interest.

We conducted a comprehensive review of experimental base pressure and base heat-transfer investigations. From the extensive data base compiled, we developed a new set of correlations that researchers in high-speed aerodynamics and flight-vehicle designers could use. This experimental data base will also be of value to researchers in computational fluid dynamics interested in validation of their computational results over a wide range of Mach number and Reynolds number. Base pressure correlations developed in this report could be applied, for example, to ballistic and maneuvering re-entry vehicles, kinetic energy penetrators, and artillery projectiles. These correlations, however, only address axisymmetric and planar geometries without thrust or base bleed and without boattails. A primary requirement for the present study was that, if possible, scaling parameters would show a clear theoretical basis and not be "invented" for convenience. In this way we could be assured of the broadest possible applicability and generality of the resulting correlations. The major effort of this study was to develop base pressure and base heat-transfer correlations for zero angle of attack. We considered laminar and turbulent boundary layers upstream of the base region as well as axisymmetric and planar geometries. Emphasis was placed on slender cones with a range of bluntness, along with wedges in planar flows. We also considered modifications of base pressure levels because of angle of attack and the specific-heat ratio of the gas.

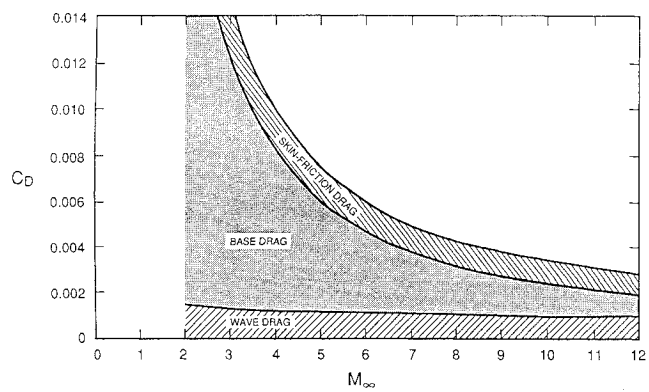

Fig. 1 Components of total drag for a slender sharp cone, θ_c = 2.9 deg.

General Description of Near-Wake Flows

To better understand the correlations developed in this report and the richness of the fluid dynamics involved, a brief description of the base flowfield will be given. An excellent summary of early theoretical developments relating to base pressure prediction is found in the review paper by Murthy and Osborn.[2] Much of the following discussion is abstracted from this article. Figure 2 schematically illustrates some of the flow features in the near wake of a blunt cone at hypersonic speeds. As the base pressure is less than the pressure in the approach flow, the viscous shock layer expands around the shoulder, forming free shear layers that coalesce at the wake neck. A velocity profile defect characterizes the wake neck region, which continues downstream as the viscous wake region. A portion of the shear-layer flow must be recirculated to satisfy continuity requirements, thus producing a toroidal vortex pattern that is adjacent to the base of the cone. A complex inviscid wave structure often includes a lip shock (associated with the corner expansion) and a wake shock (adjacent to the shear-layer confluence). At very high Mach numbers, these wave patterns often interact with each other.

Figure 3 shows a spark shadowgraph[3] of a 9-deg-half-angle cone with a sharp nose at a Mach number of 4.81. This excellent photograph reveals many detailed features of the flow in the shock layer and the turbulent flow in the boundary layer and base region. (It was taken in Ballistic Range K in the von Kármán Gas Dynamics Facility, Air Force Arnold Engineering Development Center. The test gas was air, V_∞ = 5450 ft/s, D_b = 1.75 in., P_∞ = 14.2 lb/in.^{2}, T_∞ = 75°F.) For analysis, the base flow is generally divided into four major components that exist in the near wake: corner expansion, free shear layer, recompression zone, and recirculating flow region (Fig. 4). The corner expansion process is a modified Prandtl-Meyer pattern distorted by the presence of the approaching boundary layer. A Stokes-like flowfield in the immediate vicinity of the corner allows the flow to expand (as it turns the corner) to a pressure lower than the base pressure. As the flow breaks away from the base plane, it is brought back to the base pressure by a weak shock wave known as the "lip shock"; downstream from the lip shock, the free shear layer begins to form. Figure 3 shows how the lip shock emerges from the shear layer and propagates downstream at an angle near the cone half angle.

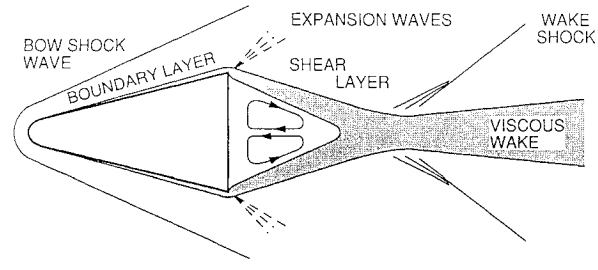

Fig. 2 Representation of flow features of a blunted cone in free flight at supersonic/hypersonic speeds.

A free shear layer (in contrast to a boundary layer) is characterized by nearly zero velocity derivatives (shear stresses) at each edge of the layer. The maximum stress occurs near the center of the shear layer. Also near the center of the layer is a "dividing" (or separating) streamline that separates that portion of the flow that originated in the approaching boundary layer from the portion that was entrained by the shear stress acting along the dividing streamline. As free shear layers from the two corners coalesce near the vehicle centerline, a region of increasing pressure (i.e., recompression) results. For cases where no mass is injected into or removed from the base region, the dividing streamline eventually results in a wake stagnation point on the centerline.

The resulting wake stagnation point marks the downstream extent of the recirculation region, because the mass entrained by the free shear layers must be reversed to flow back toward the cone base. Thus, the base plane experiences a stagnation-point flow. We know that reverse-flow velocities near the wake stagnation point are as high as 30% of the freestream velocity exterior to the shear layer. Reverse-flow Mach numbers are typically less than 0.5, but can be as high as sonic for slender cones at certain hypersonic freestream conditions.[4] However, as this reverse flow approaches the base plane, maximum velocities near the centerline become much lower. For turbulent wakes, mean values of fluctuation velocities near the base plane compare in size to the mean velocity, i.e., there is extremely high turbulence intensity. In contrast to the base pressure, the relatively low velocities adjacent to the base plane significantly affect the level of base-plane heat convection.

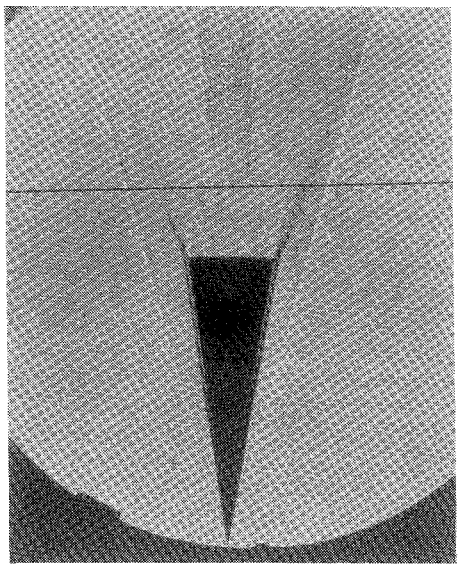

Fig. 3 Shadowgraph of a sharp cone, θ_c = 9 deg, near zero angle of attack, at a Mach number of 4.81.

Figure 4 suggests that the base plane sees a modified stagnation-point flow. Although the base-plane pressure at the stagnation point is slightly higher than the base static pressure, the maximum increase in pressure and its lateral extent are commonly small because of the low velocities in the recirculating zone. Therefore, the static pressure in the base region is usually taken as the "base pressure." Downstream of the wake stagnation point is the "wake neck," representing the minimum lateral extent (i.e., diameter) of the viscous region that originated with the boundary layers on the conical surfaces.

If we could make accurate and efficient theoretical or numerical predictions of the recirculation flow characteristics, we could determine base pressure and base heating levels. The theoretical difficulty is a result of the "free interaction" nature of the near-wake flowfield. The recirculation region is a subsonic, variable-pressure flow, elliptic in its mathematical character, while the supersonic external flow, hyperbolic in character, and contains complex wave patterns. In contrast, downstream of the wake neck, the far-wake flow, is a unidirectional flow, which is typically supersonic.

Despite the foregoing similarities, significant quantitative differences exist between near-wake flows with laminar shear layers and those with turbulent shear layers. For a given base diameter, the growth (or spread) rate of the free shear layers determines the location at which the two layers begin to interfere with each other. This point of initial interference marks the beginning of the recompression zone and determines the length scale of the near wake. Virtually all theoretical predictions and most experiments identify two flow regimes: 1) a low-Reynolds-number regime in which the shear layers are laminar at least as far downstream as the wake neck, and 2) a high-Reynolds-number regime in which the shear layers are turbulent as far upstream as the corner (or shoulder). The inclusion of laminar-to-turbulent transition within the near-wake region is an additional complication that has rarely been explored. The early work of Chapman et al.[5] indicates some major features of transitional near wakes.

Traditional wind-tunnel tests have used models supported from the rear by slender sting mounts. While such an arrangement is satisfactory for obtaining forebody flow data, it is not suited for accurately measuring base pressure variations. The presence of a sting support, no matter how small in diameter, completely destroys the structure of the shear-layer confluence at the wake neck. The strong interactions that occur at the wake neck, in free flight, contain the primary physical mechanisms that determine the base pressure.

Numerous experimental studies have erroneously concluded that because the base pressure stabilized at a constant value when the sting was decreased in diameter, support interference was negligible. Although a constant base pressure was achieved, it was not the same value as would have been measured without the sting. Even for a sting diameter of "zero," the boundary condition on the sting is a no-slip condition; without a sting, the boundary condition at the centerline is a zero radial gradient. During this study we emphasized test data obtained without rear supports. For axisymmetric bodies, such support-free data are obtained not only with actual flight tests but also in wind tunnels with free-flight model injection

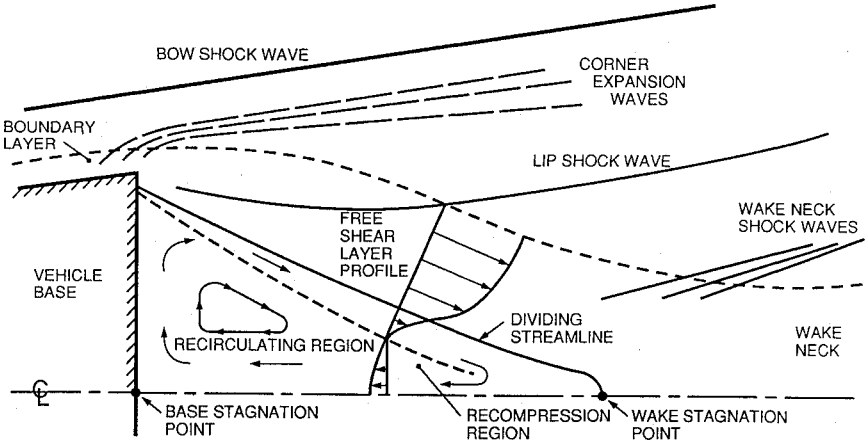

Fig. 4 Schematic of base flow features.

systems, magnetic support mechanisms, thin wire supports, or side-strut mounts.

Review of Correlation Parameters

The pioneering study of Chapman[6] included cones, ogives, cone-cylinders, ogive-cylinders, and wedges at low supersonic Mach numbers. For laminar boundary layers, he was able to correlate base pressures for different geometries using the parameters C_{pb} and $(L/H)(R_L)^{-\frac{1}{2}}$, where L is the body length, H is the base height or base radius, and R_L is the Reynolds number based on body length. This Reynolds number parameter is known to be proportional to the trailing-edge boundary-layer thickness δ/H. In this study Chapman did not attempt to correlate the effect of freestream Mach number. For cylindrical afterbodies the characteristic Mach number for both pressure coefficient and Reynolds number was the value just before separation. For cones he used a hypothetical axial Mach number that would exist if the cone (or wedge) flow were expanded to the approach flow (axial) direction. He also demonstrated that, for the thin boundary layers in his experiments, the base pressure in turbulent flow is essentially independent of the Reynolds number and thus, by implication, is a function primarily of the Mach number.

Another early study by Kurzweg[7] included cone-cylinders at Mach numbers up to 3 with laminar and turbulent boundary layers. Results were presented as P_b/P_∞ vs Reynolds number (based on body length); no attempt was made to correlate Mach-number effects. Kavanau[8] found, by trial and error, that his data for laminar flow over cones could be correlated with P_b/P_∞ vs $R^{\frac{1}{2}}/M^2$, where both Mach number and Reynolds number were based on freestream conditions. Kavanau stated that there was no obvious theoretical reason why the second power of the Mach number was successful for correlation. Lehnert and Schermerhorn[9] were the first investigators to use local shoulder (i.e., just before the base plane) parameters (P_e, M_e) for scaling cone base pressures. They obtained data for 10-deg cones with sharp and blunt noses for smooth and rough surfaces. They presented data in the form of a base pressure ratio vs a Reynolds number based on the boundary-layer momentum thickness.

Lockman[10] conducted tests on 10- and 15-deg cones at $M_\infty = 14$ and relatively low Reynolds numbers. He also correlated data with local shoulder conditions. However, he used $M_e(R_{e,s})^{-\frac{1}{2}}$ to correlate P_b/P_∞. His reason for using this particular flow parameter was its proportionality to the Knudsen number. Murman[11] used three exponents ($n = 1, 2, 3$) for the parameter $M_\infty^n(R_{\infty,s})^{-\frac{1}{2}}$ in attempting a correlation. He found that $n = 3$ (i.e., the value yielding the hypersonic interaction parameter) resulted in the best correlation of laminar base pressures on 9- and 10-deg cones at Mach numbers between 8 and 20.

Bulmer's[12] extensive study of laminar base pressures on slender cones explored the use of an effective cone Reynolds number. This Reynolds number, R_{ef}, was formed by multiplying the usual cone Reynolds number, raised to the 0.9 power, by the geometric parameter $(s/r_b)^{0.1}$. Data were plotted as $(P_b/P_\infty)(R_{ef})^{-1}$ vs R_{ef}. Also explored were correlations of P_b/P_∞ and P_b/P_e vs R_{ef}, and P_b/P_e vs a theoretical parameter developed by Reeves and Buss.[13] Their parameter has the form

$$M_e(T_e/T_0)^{\frac{3}{2}}R^{-1}(1 + 4h_w/H_e)^{-\frac{3}{2}}$$

where R is based on the shoulder properties and base radius, h_w is the enthalpy at the wall, and H_e is the total enthalpy at the edge of the boundary layer at the shoulder.

A correlation study by Kawecki[14] included both laminar and turbulent flow over cones. For laminar boundary layers his correlation used the ratio P_b/P_∞ modified by a function of M_e and the ratio of nose to base radius. This function of Mach number, pressure, and geometry was plotted vs a Reynolds number based on cone surface length and edge properties. Kawecki used the same Reynolds-number parameter to correlate turbulent flow data using P_b/P_∞. Also, Starr[15] correlated base pressure, P_b/P_∞, for cones using an effective Mach number that was a weighted function of the bluntness ratio and three reference values of the Mach number: the freestream value, the shoulder value, and a hypothetical downstream axial-flow value.

Development of New Correlation Parameters

Although a wide variety of correlation parameters has been used, we know from the previous work that a base pressure parameter is usually correlated against a flow parameter. The general form of the base pressure parameter can be written as

$$\frac{P_b}{P_{\text{ref}}} f(M) \tag{1}$$

For laminar boundary layers the flow parameter will be a function of Mach number and Reynolds number, whereas for turbulent boundary layers it will be Mach number *or* Reynolds number. Also, flow conditions used before separation generally have been more successful in correlations than freestream conditions. The flow conditions before separation contain the history of the flow processes on the vehicle—for example, nose bluntness effects and boundary-layer thickness. Laminar and turbulent flows require different sets of scaling parameters because of the fundamental differences in the effects of Mach number and Reynolds number on the development of free shear layers in the two regimes. As noted earlier, the shear layer structure is important for the base pressure level.

The traditional base pressure coefficient used in both compressible and incompressible flow is defined as

$$C_{pb} = \frac{P_\infty - P_b}{P_\infty} \frac{1}{(\gamma/2)M_\infty^2} \tag{2}$$

Comparing this with the general form of the base pressure parameter given above, we find that $P_{\text{ref}} = P_\infty$, and $f(M) = M^{-2}$ is the scaling function of Mach number. However, in the hypersonic regime, large values of the Mach number in the denominator of this equation tend to mask small variations in the base pressure ratio P_b/P_∞. Frequently, such small variations indicate important physical mechanisms. Thus, we should consider velocity parameters other than the Mach number.

Basic texts in compressible flow usually include four common dimensionless velocities for a perfect gas:

$$M = \frac{V}{a} = \frac{V}{(\gamma RT)^{\frac{1}{2}}} = \frac{V}{[\gamma RT_0(T/T_0)]^{\frac{1}{2}}}$$

$$M^* = \frac{V}{a^*} = \frac{V}{(\gamma RT^*)^{\frac{1}{2}}} = \frac{V}{[\gamma RT_0(T^*/T_0)]^{\frac{1}{2}}}$$

$$M_0 = \frac{V}{a_0} = \frac{V}{(\gamma RT_0)^{\frac{1}{2}}}$$

$$C = \frac{V}{V_{\max}} = \frac{V}{(2C_pT_0)^{\frac{1}{2}}} = \frac{V}{\left[\gamma RT_0\left(\frac{2}{\gamma - 1}\right)\right]^{\frac{1}{2}}} \tag{3}$$

The last ratio is often called the "Crocco number," in honor of the distinguished gasdynamicist L. Crocco. These defining relations show that for constant T_0, Crocco number is related linearly to local velocity. In contrast, the velocity–Mach-number relationship is nonlinear because the value of T/T_0 is itself a function of Mach number and therefore of velocity.

To investigate the upper limits of these four dimensionless velocities, we express the temperature ratio T/T_0 in terms of each velocity ratio. Thus,

$$\frac{T}{T_0} = \left(1 + \frac{\gamma - 1}{2}M^2\right)^{-1}$$

$$= 1 - \frac{\gamma - 1}{\gamma + 1}M^{*2}$$

$$= 1 - \frac{\gamma - 1}{2}M_0^2$$

$$= 1 - C^2 \tag{4}$$

In the limit as $M \to \infty$, $T/T_0 \to 0$. Therefore, for fixed T_0,

$$M^* \to \left(\frac{\gamma+1}{\gamma-1}\right)^{\frac{1}{2}} \qquad (M^* = 2.45 \quad \text{for} \quad \gamma = 1.4)$$

$$M_0 \to \left(\frac{2}{\gamma-1}\right)^{\frac{1}{2}} \qquad (M_0 = 2.24 \quad \text{for} \quad \gamma = 1.4)$$

$$C \to 1 \qquad (\text{for any } \gamma)$$

If we choose M^*, M_0, or C as a scaling parameter, the resulting numerical values will be bounded. Hence, when used as reference parameters, they will not mask small variations in base pressure ratio at high Mach numbers. One notes from Eq. (4) that the Crocco number can be computed easily for adiabatic perfect-gas flow using

$$C = [1 - (T/T_0)]^{\frac{1}{2}}$$

This relation can be expressed in terms of the Mach number as

$$C = \left(\frac{(T_0/T) - 1}{T_0/T}\right)^{\frac{1}{2}} = \left(1 + \frac{2}{\gamma-1}M^{-2}\right)^{-\frac{1}{2}} \tag{5}$$

Because the Crocco number varies between zero and unity, it is an attractive scaling parameter for the base pressure ratio P_b/P_{ref}, which also varies between zero and some small positive value. Consequently, we have used the Crocco number extensively in this study, although final correlation results are expressed in terms of Mach number for convenience.

As noted in the review of the literature, the usual flow parameter for laminar flow correlations is

$$M^n R^{-\frac{1}{2}} \tag{6}$$

where n is 1, 2, or 3. The fact that various exponents for the Mach number have been used for different sets of data suggests that the selection of a value of n was based on an inspection of the accuracy of the resulting correlation. A more general and theoretically sound approach would be to examine a simplified analysis of laminar-boundary-layer compressibility effects. The most direct approach begins with the usual Lees-Dorodnitsyn transformation[16] of the laminar-boundary-layer equations in the form

$$\xi(s) = \int_0^s \rho_e u_e \mu_e r_b^2 \, ds$$

$$\rho_e u_e r_b (2\xi)^{-\frac{1}{2}} y = \int_0^\eta \frac{\rho_e}{\rho} \, d\eta$$

where ξ and η are boundary-layer similarity variables and r_b is the body radius. Integrating the last equation across the boundary layer for the case of an external flow, with no pressure gradients, yields the following expression:

$$\frac{\delta}{s} R_{e,s}^{\frac{1}{2}} = \sqrt{2} \int_0^{\eta_e} \frac{\rho_e}{\rho} \, d\eta = f\left(M_e, \frac{T_w}{T_{0,e}}\right)$$

Solutions for the velocity profiles for various edge Mach numbers and wall temperature ratios are plotted in most advanced texts.[17] From these velocity distributions we can make estimates of the left side of the above equation, which, when plotted vs Mach number, show that for M_e greater than 3, the data are correlated when the exponent for M_e is approximately 2. That is,

$$\frac{\delta}{s} R_{e,s}^{\frac{1}{2}} \sim M_e^2 \quad \text{or} \quad \frac{\delta}{s} \sim M_e^2 R_{e,s}^{-\frac{1}{2}}$$

for each $T_w/T_{0,e}$. Recalling that the Lees-Dorodnitsyn transformation applies equally well to free shear layers and boundary layers, we can expect that parameters in the near wake region can also be correlated with this Mach number-Reynolds number parameter. This result allows us to establish a theoretical basis for using

$$M_e^2 (R_{e,s})^{-\frac{1}{2}} \tag{7}$$

as a correlation parameter for the laminar base pressure.

The result for laminar flow can be contrasted with the case of turbulent wakes, in which the shear-layer growth is independent of Reynolds number. (A minor exception to this experimental observation is the small effect of the initial boundary-layer thickness before separation.) Thus, turbulent base pressures will be primarily a function of Mach number and secondarily of wall temperature ratio.

Experimental Flow Conditions and Geometries

The initial review of the literature in this study consisted of about 50 sources of experimental data. Some of the data could not be used, because they were presented only in a correlated form. Thus, we could not retrieve basic information and recast it into other correlations. For other sources of data, missing parameters also prohibited us from confidently constructing new correlations. However, for some of these cases, we could perform computations using given data and thereby infer the values of unknown parameters. Other sources of data were not used because they were narrow in the range of flow conditions, or they overlapped more extensive sets of data. We used results for sting-supported models only when necessary to include a specific range of Mach numbers or Reynolds numbers, or a certain geometry.

Table 1 summarizes flow conditions and body geometries for the eleven laminar-flow data sources included in this study. The most interesting data are Bulmer's[12] flight test results on 9-deg-half-angle cones with 5 and 6% bluntness. Additional flight data are available from Cassanto[18] on 10-deg cones with bluntness ratios up to 60%. The data of Lockman[10] using wire-supported models in a wind tunnel exhibited a systematic variation of nose blunting. Pick[19] fired free-flight sharp cones in a wind tunnel over a range of Mach number, Reynolds number, and angle of attack. Supplementing these data on spherically blunted cones are data on cylinders with various forebodies. Badrinarayanan[20] obtained data on very long cylinders, and Chapman,[6] Kurzweg,[7] and Reller and Hamaker[21] obtained data on cone-cylinders and ogive-cylinders. Few planar base pressure data are available. Batt and Kubota,[22] Chapman,[6] and Dewey[23] tested wedge half-angles between 2 deg and 22.5 deg.

Table 2 summarizes experimental parameters for 14 turbulent flow sources used in this study. Bulmer's[24] data on spherically blunted cones are foundational data because they comprise the largest range of Mach number. The data of Mark,[25] Tanner,[26] Uselton and Cyran,[27] and Zarin[28] comprise lower Mach numbers and cover the range of cone half angles from 3.4 to 9 deg. The data of Pepper and Holland[29] and Wehrend[30] contain information at very low Mach numbers and relatively large cone half angles. For cylindrical geometries with cone and ogive forebodies, we used the data of Chapman,[6] Kayser,[31] Reller and Hamaker,[21] and Moore et al.[32] Also included are the data from various wind-tunnel investigators compiled by Seiling and Page.[33] In addition, we used planar base pressure data of Goecke[34] from the X-15 flight test program and a compilation of data by McDonald.[35]

Laminar Flow Correlations

Axisymmetric Flow

Bulmer's[12] flight data are plotted in Fig. 5a using the coordinates P_b/P_e as a function of $M_e^2(R_{e,s})^{-\frac{1}{2}}$. The Reynolds number is based on boundary-layer edge fluid properties and body surface length from the stagnation point. Because the data for Mach 20 and 6% bluntness fall below the data for Mach 16 and 5% bluntness, P_e is not the most appropriate reference pressure when comparing data for different geometries or flight conditions. As previous correlations show, an alternative reference pressure is the one that would exist if the flow at the shoulder (P_e, M_e) were expanded through an angle θ_c to the axial direction. For slender sharp cones ($\theta_c < 15$ deg), simple computations show that the static pressure for a flow

Table 1 Laminar base pressure: experimental conditions

Investigator	Geometry	M_∞	$R_{\infty L}$	Test condition
Bulmer[12]	9-deg cone, $r_n/r_b = 0.05$	16	$(0.2–48) \times 10^6$	Free flight (RV)
	9-deg cone, $r_n/r_b = 0.06$	20		
Cassanto[18]	10-deg cone, $r_n/r_b = 0, 0.3, 0.6$	4	$(0.5–10) \times 10^6$	Wind tunnel (sting) Free flight (RV)
Lockman[10]	10-deg, 15-deg cones, $r_n/r_b = 0, 0.1, 0.2, 0.3, 0.4, 0.5$	14	$(2–7) \times 10^4$	Wind tunnel (wire)
Pick[19]	10-deg cone, $r_n/r_b = 0$	5.3–9.9	$(1.5–5.6) \times 10^5$	Free flight (wind tunnel)
Badrinarayanan[20]	Cylinder, $L/D = 24$	2	0.7×10^6	Wind tunnel (side strut)
Kurzweg[7]	Cone/cylinder, $L/D = 4$	3	$(0.5–3) \times 10^6$	Wind tunnel (sting)
Chapman[6]	Ogive/cylinder, $L/D = 3–7$	1.5, 2	$(0.5–2) \times 10^6$	Wind tunnel (sting)
	Cone/cylinder, $L/D = 4–9$	1.5, 2		
Reller and Hamaker[21]	Ogive/cylinder, $L/D = 5$	2.7–5	$(1.4–4) \times 10^6$	Wind tunnel (sting)
Chapman[6]	2-deg wedge	2	$(1.5–2.4) \times 10^5$	Wind tunnel (wall mount)
Batt and Kubota[22]	10-deg wedge	6.1	$(0.3–2.4) \times 10^5$	Wind tunnel (wall mount)
Dewey[23]	15-deg, 22.5-deg wedges	6	$(0.15–2.0) \times 10^5$	Wind tunnel (wall mount)

Table 2 Turbulent base pressure: experimental conditions

Investigator	Geometry	M_∞	$R_{\infty L}$	Test condition
Bulmer[24]	9-deg cone, $r_n/r_b = 0.05, 0.06$	2–15	$(2–17) \times 10^7$	Free flight (RV)
Zarin[28]	9-deg cone, $r_n/r_b = 0, 0.286$	3.5–9.2	$(0.5–10) \times 10^6$	Wind tunnel (sting)
Mark[25]	8-deg cone, $r_n/r_b = 0.01$	2–3	$(3–3.6) \times 10^7$	Wind tunnel (injection)
Uselton and Cyron[27]	6-deg cone, $r_n/r_b = 0.1, 0.15$	2–10	$(2–4) \times 10^7$	Wind tunnel (sting)
Tanner[26]	3.4-deg cone, $r_n/r_b = 0.15$	5–6.8	N/A	Wind tunnel (side strut)
Pepper and Holland[29]	15-deg cone, $r_n/r_b = 0, 0.4, 0.6$	1.3	N/A	Wind tunnel (wires)
Wehrend[30]	12-deg cone, $r_n/r_b = 0$	1.3–2.2	N/A	Wind tunnel (sting)
Chapman[6]	Cone/cylinder, $L/D = 5$	2–4	$(3–6) \times 10^6$	Free flight
Kayser[31]	Ogive/cylinder, $L/D = 6$	1.2	4.5×10^6	Wind tunnel (sting)
Reller and Hamaker[21]	Ogive/cylinder, $L/D = 10$	2.7–5	5×10^6	Wind tunnel (sting)
Seiling and Page[33]	Cylinders	1.5–4	N/A	Wind tunnel (forward support)
Moore et al.[32]	Ogive/cylinder, $L/D = 7.2$	2–4.5	6×10^6	Wind tunnel (side strut)
Goecke[34]	5-deg wedge	1.5–5	$(0.4–2) \times 10^7$	Free flight (X-15)
McDonald[35]	Wedges/backsteps	1.25–3	N/A	Wind tunnel (wall mount)

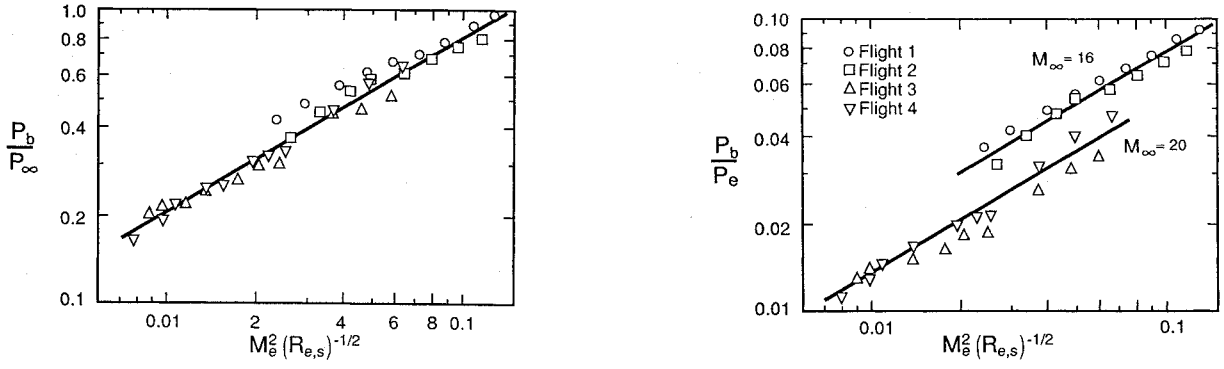

a) P_e reference pressure **b) P_∞ reference pressure**

Fig. 5 Variation of base pressure in axisymmetric laminar flow, showing effect of reference pressure.

so expanded is approximately 75% of the freestream pressure for Mach numbers between 2 and 15. The hypothesis that the axial pressure ($\approx P_\infty$) is an appropriate reference pressure is tested in Fig. 5b. This figure shows that P_b/P_∞ does brings the two sets of data into better agreement. For larger cone angles ($\theta_c > 15$ deg), the approximation that the axial pressure $\approx P_\infty$ would not be as accurate. For this case, we could obtain a more appropriate reference pressure by computing the pressure that would result from the flow passing through an Prandtl-Meyer expansion to the axial direction.

Figure 6 shows the entire set of laminar-flow data in terms of P_b/P_∞, where, for the cylinder data of Badrinaryanan,[20] P_∞ is the shoulder pressure. For this plot, edge conditions (if not reported by the investigator) were determined by taking the computational results from inviscid-flow predictions using an Euler code (SANDIAC), which has been used at Sandia National Laboratories for many years. The code has been validated for a large number of vehicle geometries and flowfields. (See Noack and Lopez,[36] McWherter et al.,[37] and Daywitt et al.[38] for additional details.)

For each M_∞, the data for a given body correlate satisfactorily (as did Bulmer's[12] cone data); however, the lower-Mach-number data are displaced upward from the hypersonic flow cases (except for the Lockman[10] data). In addition, Fig. 6 provides an indication of possible differences between data for free-flight and sting-supported

models. Cassanto's[18] flight data (symbols with flags) and those from sting-supported models indicate that the rear supports produced base pressure levels that were 25% to 50% higher than the flight data. However, these differences are generally within band of Bulmer's flight data. As Table 1 shows, the data of Lockman were obtained at a freestream Reynolds number that is approximately 100 times lower than all other data sets. The resulting low-Reynolds-number influence will be discussed shortly.

The results seen in Fig. 6 confirm earlier correlations; that is, the parameter $M_e^2(R_{e,s})^{-\frac{1}{2}}$ successfully correlates data for a variety of geometries over a small range of approach Mach numbers. Because P_b/P_∞ does not correlate data over a broad range of Mach numbers, additional scaling is required for the complex interaction of coalescing shear layers at the wake neck. As noted earlier, this coalescence is a crucial component in the determination of base pressure. The theoretical basis for this assertion is found in the early work of Reeves and Lees,[39] who showed that the wake neck is characterized by a strong interaction between the interior viscous flow (which contains regions of subsonic flow) and the external, inviscid supersonic flow.

In seeking a method of scaling P_b/P_∞, the use of the Crocco number is desirable because of its variation between zero and unity. Therefore, using a trial-and-error procedure, we can demonstrate that, by scaling the pressure ratio with

$$C_e^4 = [1 - (T/T_0)]_e^2,$$

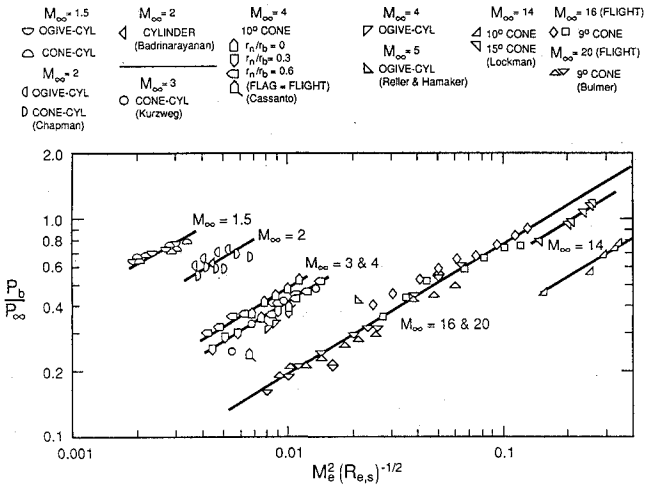

Fig. 6 Variation of base pressure in axisymmetric laminar flow for the total data set used in the present study.

all data sets (except for that of Lockman) fall along a single line (Fig. 7). The slope of the line in log-log coordinates is 0.6. Thus, the final correlation equation for axisymmetric laminar flow is given by

$$\frac{P_b}{P_\infty} C_e^4 = 3.05\left[M_e^2(R_{e,s})^{-\frac{1}{2}}\right]^{0.6} \tag{8a}$$

In terms of Mach number, the foregoing equation can be written as

$$\frac{P_b}{P_\infty} = 3.05\left(1 + \frac{2}{\gamma - 1} M_e^{-2}\right)^2 \left[M_e^2(R_{e,s})^{-\frac{1}{2}}\right]^{0.6}. \tag{8b}$$

Why were Lockman's measurements displaced from the remaining body of data? It was suspected that the root cause was the unusually low Reynolds numbers for these tests (Table 1). To investigate these conditions, a series of computations were made for Lockman's spherically blunted 10-deg cone using a parabolized Navier–Stokes code (SPRINT), which has been used at Sandia National Laboratories for several years. The code has been validated for a large number of vehicle geometries over a wide range of Mach and Reynolds number. (See Stalnaker et al.,[40] Walker and McBride,[41] and Oberkampf et al.[42] for additional details.)

The boundary-layer thickness was computed at $M_\infty = 14$ for various flight altitudes. Based on the earlier discussion concerning boundary-layer similarity variables, one suspects that the parameter $(\delta/s)(R_{e,s}^{\frac{1}{2}}/M_e^2)$ should be a simple power-law function of edge Reynolds number. As Fig. 8 shows, the trend changes at low Reynolds numbers because the boundary-layer growth becomes inversely proportional to a power of the Reynolds number greater than the usual one-half. Thus, the Lockman data can be made to coincide with the foregoing correlation equation for axisymmetric flow by using $R_e^{0.65}$ rather than $R_e^{0.5}$. Similar low-Reynolds-number effects on a flat plate in incompressible flow are discussed by White (Ref. 17, p. 266). Based on Lockman's data, the present laminar base pressure correlations are not expected to be reliable for $R_{e,s} < 10^5$.

Planar Flow

The four sets of data for planar laminar flow are shown in Fig. 9. As before, use of $M^2R^{-\frac{1}{2}}$ correlates each data set, but the base pressure ratio requires further scaling by C_e to achieve agreement between data sets. Figure 10 shows that $C_e^6 = (1 - T/T_0)_e^3$ is required for full correlation. Thus, we obtain a correlation equation in the form

$$\frac{P_b}{P_\infty} C_e^6 = \left[M_e^2(R_{e,s})^{-\frac{1}{2}}\right]^{0.6}$$

Note that the constant of proportionality comes out unity. In terms

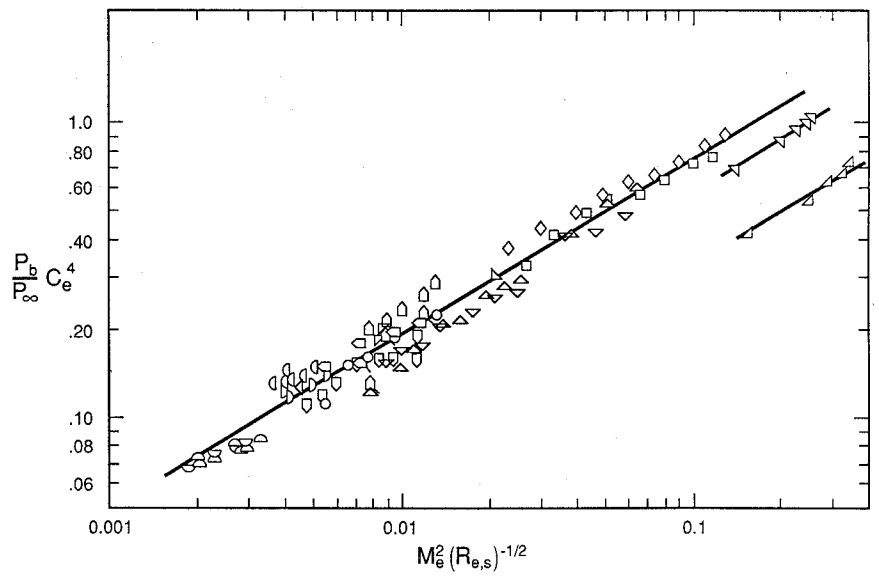

Fig. 7 Final correlation of base pressure in axisymmetric laminar flow.

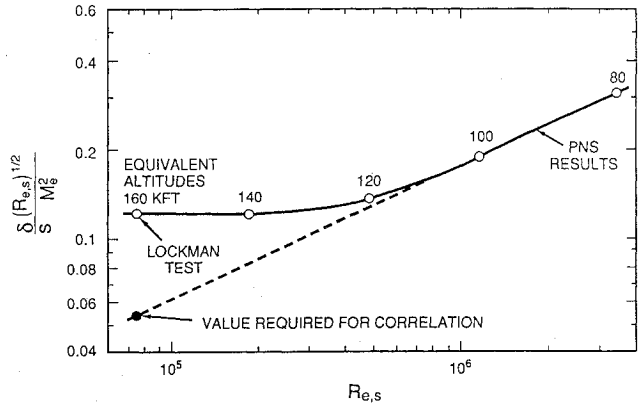

Fig. 8 Variation of laminar-boundary-layer thickness for hypersonic flow over a 10-deg cone at $M_\infty = 14$.

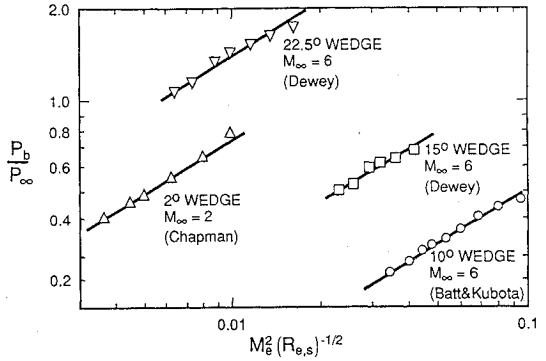

Fig. 9 Variation of base pressure in planar laminar flow for the total data set used in the present study.

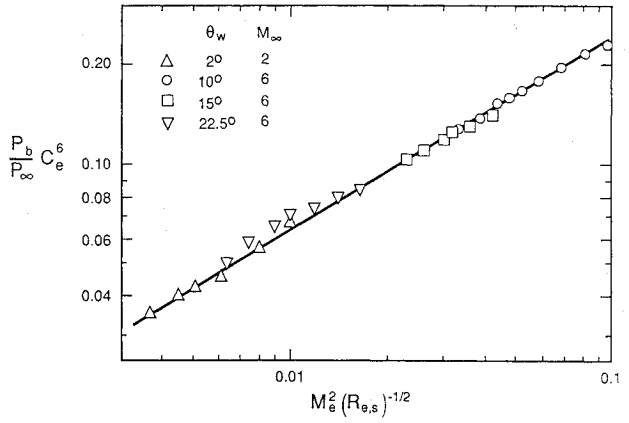

Fig. 10 Final correlation of base pressure in planar laminar flow.

of Mach number, it is

$$\frac{P_b}{P_\infty} = \left(1 + \frac{2}{\gamma - 1} M_e^{-2}\right)^3 \left[M_e^2 (R_{e,s})^{-\frac{1}{2}}\right]^{0.6} \tag{9}$$

The exponent 0.6 on the parameter $M^2 R^{-\frac{1}{2}}$ is the same for axisymmetric and planar flows, making us confident of the present approach.

The primary reason for the different powers of C_e (required to correlate axisymmetric and planar base pressures) is the different flow structures for the two geometries. As stated in the earlier discussion of near-wake structure, the interaction of converging shear layers at the wake neck largely determines the base pressure. For axisymmetric geometries, there is a strong effect of transverse curvature that is not present in planar flow. (A similar comparison is seen in inviscid solutions by the method of characteristics for axisymmetric and planar geometries.) Another distinguishing feature of base flow in the two geometries is the existence of a much larger core of subsonic flow near the centerline of an axisymmetric near wake, as compared to the centerplane of a planar wake. From this, we would expect that the effect of C_e would not be scaled the same for the two geometries.

Turbulent Flow Correlations

Axisymmetric Flow

As noted in the review of previous correlations, the effect of Reynolds number in turbulent free shear flow is quite small, because the shear layers are governed by large-scale turbulent structures. The influence of an approaching boundary layer (characterized by a specific Reynolds number) has been correlated in previous studies through the parameter θ/H, where θ is the boundary-layer momentum thickness and H is the base radius or base height in planar flow. Both Chapman[43] and Korst[44] showed theoretically that the minimum base pressure occurs when $\theta/H \to 0$. Thus, when the boundary-layer thickness increases, the base pressure is slightly increased. This consequence does not affect operational flight vehicles because such thick boundary layers typically occur only in the laminar regime. As a result, thick turbulent boundary layers are not included in this study. (For hypersonic flight conditions with large ablation and mass transfer at the surface, a turbulent boundary can become relatively thick.)

Figure 11 shows a set of data[33] for long cylinders (having no rear support) with shoulder Mach numbers M_1 between 1.5 and 4. The scatter of these data is caused by the values of larger θ/H, as noted above. This traditional presentation of turbulent-flow data shows how P_b/P_1 varies with M_1 and illustrates the problem of comparing and correlating hypersonic measurements with data from low-supersonic flows.

Use of C_1 (which is related linearly to velocity) in lieu of M_1 on the horizontal scale allows the hypersonic range to be displayed in a more physically realistic manner. Figure 12 shows the compiled data of Seiling and Page[33] and data from Chapman,[6] Kayser,[31] and Reller and Hamaker[21] plotted as P_b/P_1 vs C_1^2. The parameter C_1^2 groups the wider range of Mach-number data reasonably well. For the limit of infinite Mach number ($C_1 \to 1$), the theoretical mean line would approach the physical singularity with an infinite slope.

The correlation equation for the linear portion of the variation is given by

$$\frac{P_b}{P_1} = 0.05 + 0.967\left(1 - C_1^2\right)$$

$$= 0.05 + 0.967(T/T_0)_{M_1}$$

$$\frac{P_b}{P_1} = 0.05 + 0.967\left(1 + \frac{\gamma - 1}{2} M_1^2\right)^{-1} \tag{10}$$

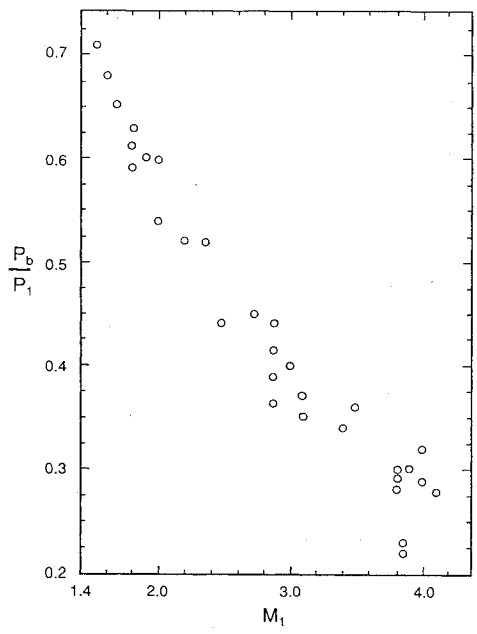

Fig. 11 Variation of base pressure for turbulent flow past long cylinders.

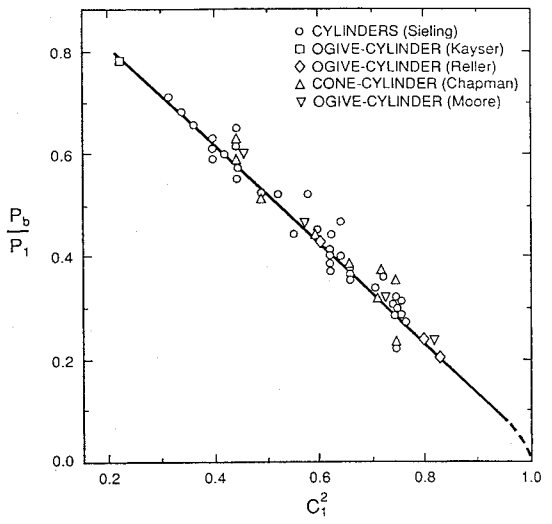

Fig. 12 Correlation of base pressure for turbulent flow over cylinders.

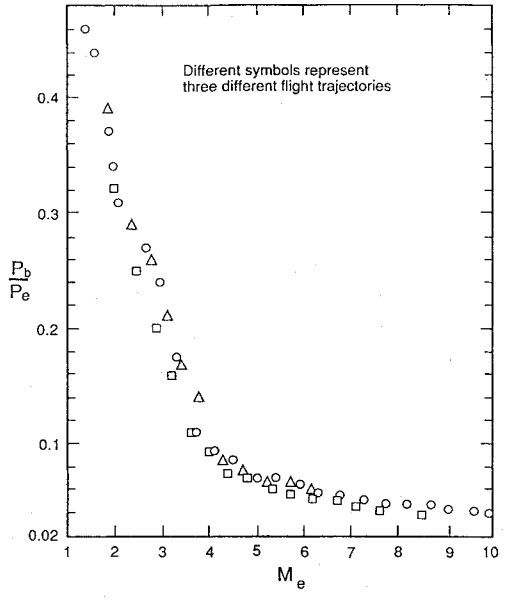

Fig. 13 Variation of base pressure for turbulent flow over blunted 9-deg cones using shoulder reference conditions.

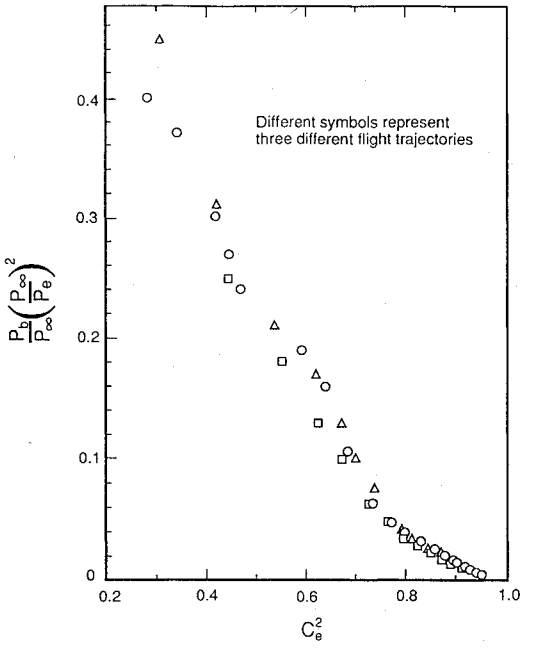

Fig. 14 Variation of scaled base pressure for turbulent flow over cones using shoulder reference Crocco number.

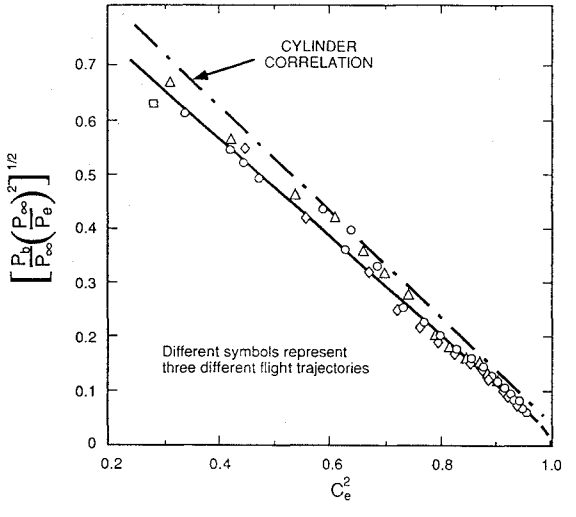

Fig. 15 Correlation of base pressure in axisymmetric turbulent flow over cones using edge conditions for reference.

It is seen that the intercept of the above equation for $C_1 = 1$ is 0.05. For values of C_1 above 0.98 ($M_1 > 15$), one should take account of the curvature of the correlation curve (dashed line).

Is it possible to scale base pressures for cones in such a way as to correlate them with the cylinder data? Because Bulmer's[24] flight-test data for $\theta_c = 9$ deg form the most complete set of turbulent hypersonic base pressure data available, they were used for the initial part of this phase. He attempted to correlate his base pressure data using the coordinates P_b/P_∞ vs M_∞. The resulting distributions exhibited a surprising double-valuedness; i.e., two values of M_∞ can produce the same P_b/P_∞ value. Some improvement was obtained when edge conditions at the cone shoulder (P_e and M_e) were used as scaling parameters, i.e., P_b/P_e. Insight into the variation of the ratio P_b/P_e can be obtained by expressing it in terms of the original ratio P_b/P_∞. Thus, we have

$$\frac{P_b}{P_e} = \frac{P_b}{P_\infty}\left(\frac{P_e}{P_\infty}\right)^{-1}$$

As shown in Fig. 13, the resulting variation has no double values but does exhibit a sharp "knee," which would be difficult to correlate successfully. During this investigation, we attempted to do this, but we were only partially successful. We also realized that the knee occurs because the upward trend of P_b/P_∞ at high Mach numbers tends to partially cancel the corresponding decrease in the ratio P_∞/P_e. Conditions at which the knee occurs are not universal, but are related to the nose bluntness and cone angle. As the upward trend of P_b/P_∞ is partially cancelled by normalizing with P_e/P_∞, we suspect that additional improvement could be attained by using $(P_e/P_\infty)^2$ as a normalizing parameter for P_b/P_∞. Thus, we can plot Bulmer's data using the base pressure ratio

$$\frac{P_b}{P_\infty}\left(\frac{P_e}{P_\infty}\right)^{-2} = \frac{P_b}{P_e}\frac{P_\infty}{P_e}$$

The Euler code SANDIAC was used to generate values of P_e/P_∞, M_e, and C_e (Figs. 14 and 15). As with cylinders, the parameter M_e (Fig. 13) was replaced by C_e^2. The resulting distribution (Fig. 14) of the modified base pressure parameter as a function of C_e^2 displays little effect of the knee at higher values of M_e (or C_e^2). This distribution also suggests that a fractional power of the pressure parameter would reduce the curvature and thus could yield the desired linear variation. For the case of $\theta_c = 9$ deg (Fig. 14), the exponent

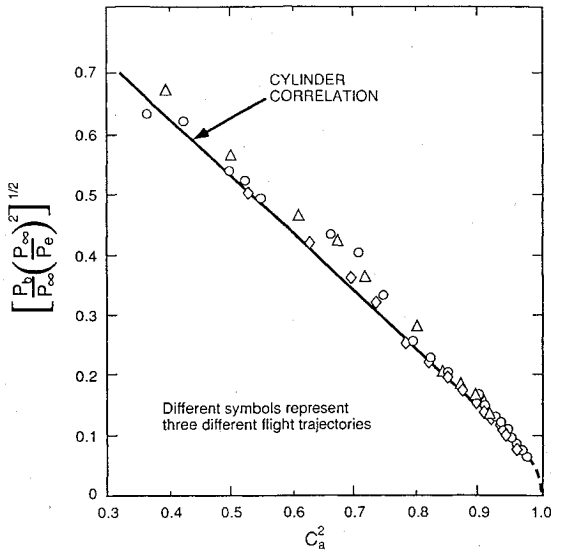

Fig. 16 Correlation of base pressure in axisymmetric turbulent flow using axial flow conditions for reference.

was approximately one-half, as indicated in Fig. 15, which shows

$$\left[\frac{P_b}{P_\infty}\left(\frac{P_e}{P_\infty}\right)^{-2}\right]^{\frac{1}{2}}$$

as a function of C_e^2. It is also seen in Fig. 15 that the cone base pressure distribution lies somewhat below the cylinder correlation of Fig. 12.

However, to bring these two curves into congruence, it is necessary to recall that, for laminar flow, the pressure in a hypothetical axial flow downstream of the cone shoulder was a satisfactory reference pressure (Fig. 5). Similar reasoning can be used for comparing cylinders and cones in turbulent flow. Thus, the axial Crocco number, C_a^2, is expected to play the same role as C_1^2 for cylinders. The value of C_a^2 is determined by the relation

$$\nu_a(C_a^2) = \nu_e(C_e^2) + \theta_c$$

where ν is the Prandtl-Meyer angle and θ_c is the cone half angle.

A replot of the flight data of Fig. 15 in terms of C_a^2 is shown in Fig. 16. This figure shows that the two correlations (cylinder and cone) of Fig. 15 are brought into congruence, which also implies that the near-wake structure for the two congruent cases will be very similar.

Although the exercise of using C_a^2 provides confidence in the generality of the present correlation scheme, a more direct working correlation would use C_e^2. The solid-line correlation shown in Fig. 15 is given by the following equation:

$$\left[\frac{P_b}{P_\infty}\left(\frac{P_\infty}{P_e}\right)^2\right]^N = 0.025 + 0.906(1 - C_e^2)$$

or

$$\frac{P_b}{P_\infty} = \left(\frac{P_e}{P_\infty}\right)^2\left[0.025 + 0.906\left(1 + \frac{\gamma - 1}{2}M_e^2\right)^{-1}\right]^{1/N}$$

where $N \approx 0.5$ for $\theta_c = 9$ deg.

Unfortunately, extensive data for cone angles other than 9 deg are not available. However, for the limited information available for other cone angles, it was found that the exponent N takes a different value for each θ_c. Data for a range of cone half angles are plotted in Fig. 17, which includes the same correlation line as in Fig. 15 (also given above). Thus, the final correlation equation for cones is

$$\frac{P_b}{P_\infty} = \left(\frac{P_e}{P_\infty}\right)^2\left[0.025 + 0.906\left(1 + \frac{\gamma - 1}{2}M_e^2\right)^{-1}\right]^J \qquad (11)$$

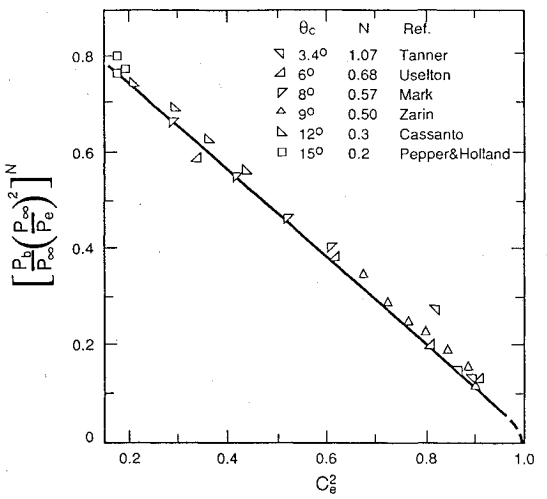

Fig. 17 Correlation of base pressure for turbulent flow past cones of various angles.

where

$$J = \frac{1.7}{\ell n(21/\theta_c)}$$

where θ_c is in degrees.

The exponent J cannot be used for $\theta_c > 20$ deg; therefore, we must consider this correlation to be valid for slender cones only. For larger cone angles, we would expect the character of the near-wake flow to be considerably different from that shown in Figs. 3 and 4. In particular, as θ_c increases, the Mach number at the edge of the boundary layer will decrease markedly. In addition, the corner expansion process will become much more prominent because of the larger turning angles and a stronger interaction with the outer portions of the shock layer. Therefore, we would expect that the base pressure would have virtually no relationship to the cone surface flow parameters M_e and C_e. Entirely different scaling parameters would be required. The lack of systematic data for large-angle cones precluded work in this area. However, the experimental results of McAlister et al.[45] suggest that the value of C_{p_b} [Eq. (2)] becomes constant for very large cone angles at hypersonic speeds.

Planar Flow

The variation of base pressure in planar turbulent flows is similar to that shown in Fig. 11 for cylinders; that is, the value of P_b decreases with increasing Mach number upstream of the base plane. Following the same procedure as in axisymmetric flow, we can plot a base pressure ratio vs either C_a or C_a^2. The correlation is shown in Fig. 18, which includes data for both wedges and backsteps. Unlike cylinder flows, a linear relation is obtained when the planar base pressure ratio is plotted vs C_a rather than C_a^2. For backsteps, P_∞ and C_a represent the freestream flow upstream of the corner, whereas for wedges, these two parameters represent a hypothetical axial flow downstream of the corner. As with the cylinder data, much of the scatter is due to boundary-layer effects before separation, which were manifested as widely varying values of δ/H. The equation for this correlation line is

$$\frac{P_b}{P_\infty} = 0.01 + 1.03(1 - C_a) \qquad (12)$$

Base Heat Transfer for Axisymmetric Bodies

It is well known that convection heat transfer can be correlated using either the Stanton or the Nusselt number. A characteristic Nusselt number for the base plane can be written as

$$Nu_b = \frac{\tilde{h}_b r_b}{k_b}$$

where $\tilde{h}_b$ is the convective heat-transfer coefficient and k_b is the thermal conductivity of the gas. Likewise, the base Stanton number

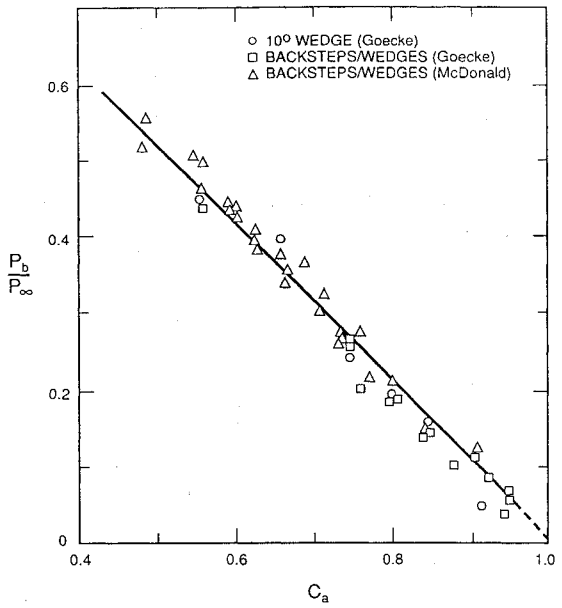

Fig. 18 Correlation of base pressure in planar turbulent flow using axial flow conditions for reference.

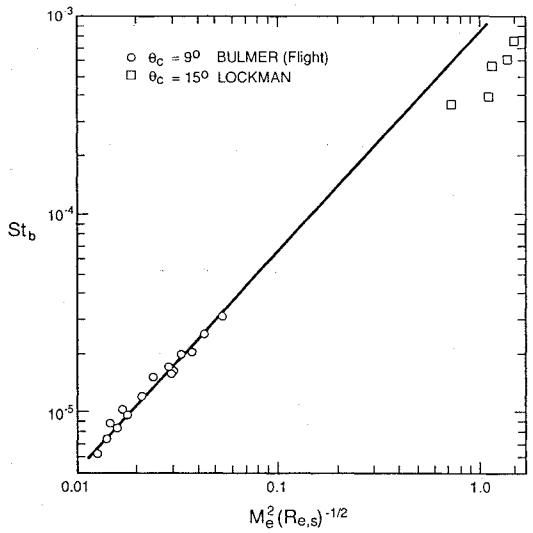

Fig. 19 Variation of base Stanton number with correlation parameter for laminar flow over cones.

can be expressed as a ratio of two convective heat transfer rates. Thus,

$$St_b = \frac{\dot{q}_b}{\dot{q}_{\text{ref}}} = \frac{\dot{q}_b}{\rho_\infty u_\infty (H_\infty - h_w)}$$

where H_∞ is the freestream stagnation enthalpy and h_w is the static enthalpy. Unlike the Nusselt number, the base Stanton number does not include the size of the base surface or any fluid properties other than density. Thus, the Stanton number is the preferred parameter for base heating. In particular, the lack of a length scale in the Stanton number allows us to use a Reynolds number with unit length—or, preferably, the unit Reynolds number R'—for correlation. (These two parameters have the same value, but only the Reynolds number is nondimensional.) Thus, we can write

$$St_b = f(R'_b) \tag{13}$$

to express a base heating correlation, where $R'_b = (\rho u/\mu)_b$.

It is possible to greatly simplify the correlation of base convection by relating the base-plane unit Reynolds number to the base pressure. Comparing the values of R' on the base and in the edge flow adjacent to the shoulder shows that

$$R'_b = R'_e \frac{\rho_b}{\rho_e} \frac{\mu_e}{\mu_b} \frac{u_b}{u_e}$$

where $R'_e = (\rho u/\mu)_e$. First recall that velocity is linearly related to Crocco number. Therefore, using the viscosity approximation $\mu \propto T^\omega$ allows us to write the above equation as

$$R'_b = R'_e \frac{P_b}{P_e} \left(\frac{T_e}{T_b}\right)^{1+\omega} \frac{C_b}{C_e} \left(\frac{T_{0b}}{T_{0e}}\right)^{\frac{1}{2}}$$

Because recirculation velocities are small, C_b is much less than C_e, and therefore $T_b = T_{0b}$. Also, in the absence of significant heat transfer across the shear layer, the approximation, $T_{0b} \approx T_{0e}$ can be made. Thus, we can write

$$\frac{T_e}{T_b} = \frac{T_e}{T_{0e}} \frac{T_{0e}}{T_{0b}} \frac{T_{0b}}{T_b} = \frac{T_e}{T_{0e}} = F(M_e)$$

The fundamental nature of the recirculating flowfield suggests that because u_b (or C_b) remains nearly constant over a wide range of C_e values, it can be removed from further consideration. Therefore, the relation between the two unit Reynolds numbers becomes

$$R'_b \sim R'_e \frac{P_b}{P_e} F(M_e) C_e^{-1} \tag{14}$$

This shows that the characteristic base-plane unit Reynolds number and the base Stanton number are functions of base pressure ratio, edge Mach number, and edge Reynolds number. However, in the foregoing base pressure correlations, we already have developed relationships between the latter three parameters. This result suggests that the same parameters that correlated the base pressure might be used to correlate the base Stanton number.

As demonstrated in the following section, this supposition is true for laminar flow. Thus, for laminar flow cases,

$$St_b = f\left[M_e^2 (R_{e,s})^{-\frac{1}{2}}\right] \tag{15}$$

However, for the turbulent flow regime St_b is only a function of M_e, since the Reynolds number plays no significant role.

Unfortunately, there are few test data for base heat transfer, because such measurements are more difficult to make than the corresponding pressure measurements. Bulmer's[46,47] flight measurements on 9-deg cones (in both laminar and turbulent regimes) form the primary set of data to be correlated.

Laminar Flow

Shown in Fig. 19 are Bulmer's laminar flight data for 9-deg cones with Lockman's[10] measurements on 15-deg cones with blunting from zero to 40%. Lockman's data fall below the correlation line for Bulmer's data, just as did the corresponding pressure measurements (Fig. 7). As explained earlier, the problem is the low-Reynolds-number conditions that led to a different exponent of the Reynolds number.

The correlation line of Fig. 19 is given by the expression

$$St_b = 8.0 \times 10^{-4}\left[M_e^2 (R_{e,s})^{-\frac{1}{2}}\right]^{1.1}$$

Recall the correlation of base pressure from Fig. 8, Eq. (8a), as

$$\frac{P_b}{P_\infty} C_e^4 = 3.05\left[M_e^2 (R_{e,s})^{-\frac{1}{2}}\right]^{0.6}$$

We can eliminate the parameters M_e and R_e in the brackets from these equations and obtain a correlation for Stanton number in terms of base pressure. This correlation is shown in Fig. 20 and can be expressed as

$$St_b = 1.0 \times 10^{-4}\left(\frac{P_b}{P_\infty} C_e^4\right)^{1.8} \tag{16}$$

Writing this in terms of M_e, we have

$$St_b = 1.0 \times 10^{-4}\left[\frac{P_b}{P_\infty}\left(1 + \frac{2}{\gamma - 1} M_e^{-2}\right)^{-2}\right]^{1.8} \tag{17}$$

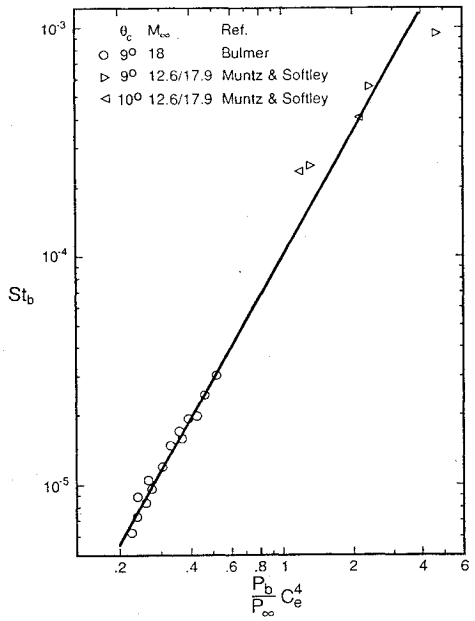

Fig. 20 Correlation of base Stanton number with base pressure parameter for laminar flow over cones.

Figure 20 shows the correlation of Stanton number with base pressure in Eq. (16). Also shown in the figure are two additional data sets of Muntz and Softly,[48] which were compiled by Bulmer. These data encompass cone angles of 9 and 10 deg, with Mach numbers of 12.6 and 18, and bluntness ratios of 0.05 and 0.3.

Turbulent Flow

Bulmer's turbulent heat-transfer measurements, converted to Stanton number, are shown in Fig. 21. The correlation line given in Fig. 21 is expressed as

$$St_b = 8.3 \times 10^{-4}\left\{\left[\frac{P_b}{P_\infty}\left(\frac{P_\infty}{P_e}\right)^2\right]^{\frac{1}{2}}\right\}^{1.85} \tag{18}$$

The correlation is satisfactory for the very limited data available, i.e., for a single-cone geometry. Before a comprehensive correlation can be developed, additional data are required for various cone angles, bluntness ratios, and Mach numbers. This equation could be used to make estimates of convection levels for other values of θ_c between 6 and 12 deg. However, in the interim, we could make estimates of convection levels for other cone angles by replacing the one-half power of the bracketed pressure terms in Eq. (18) with the exponent J^{-1}, which is defined in conjunction with Eq. (11).

For easy reference, Table 3 gives a compilation of all the correlations developed in this study for zero angle of attack.

Table 3 Summary of correlations for zero angle of attack

	Laminar
Axisymmetric	$\frac{P_b}{P_\infty} = 3.05\left(1+\frac{2}{\gamma-1}M_e^{-2}\right)^2\left[M_e^2(R_{e,s})^{-\frac{1}{2}}\right]^{0.6}$
Planar	$\frac{P_b}{P_\infty} = \left(1+\frac{2}{\gamma-1}M_e^{-2}\right)^3\left[M_e^2(R_{e,s})^{-\frac{1}{2}}\right]^{0.6}$
Cone	$St_b = 1.0\times10^{-4}\left[\frac{P_b}{P_\infty}\left(1+\frac{2}{\gamma-1}M_e^{-2}\right)^{-2}\right]^{1.8}$
	Turbulent
Cylinder	$\frac{P_b}{P_1} = 0.05+0.967\left(1+\frac{\gamma-1}{2}M_1^2\right)^{-1}$
Cone	$\frac{P_b}{P_\infty} = \left(\frac{P_e}{P_\infty}\right)^2\left[0.025+0.906\left(1+\frac{\gamma-1}{2}M_e^2\right)^{-1}\right]^J$ where $J=\frac{1.7}{\ln(21/\theta_c)}$ and $\theta_c \le 20$ deg
Planar	$\frac{P_b}{P_\infty} = 0.01+1.03\left\{1-\left[1-\left(1+\frac{\gamma-1}{2}M_a^2\right)^{-1}\right]^{\frac{1}{2}}\right\}$
Cone	$St_b = 8.3\times10^{-4}\left\{\left[\frac{P_b}{P_\infty}\left(\frac{P_\infty}{P_e}\right)^2\right]^{\frac{1}{2}}\right\}^{1.85}$

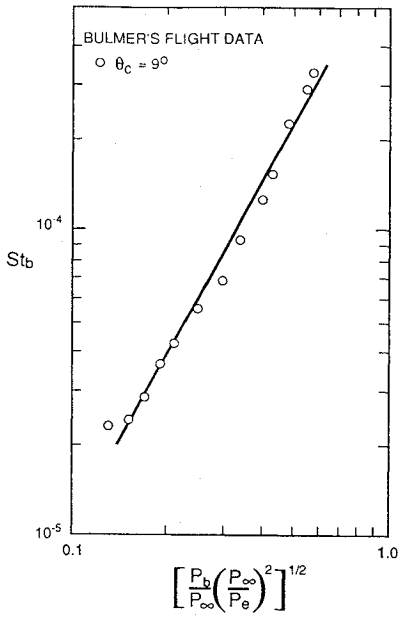

Fig. 21 Correlation of base Stanton number for turbulent flow over a blunted 9-deg cone.

Angle-of-Attack Effects

When a body of revolution is inclined to the freestream direction, the result is a highly three-dimensional flowfield over the body surface and in the wake region. In such flows, the difficulties of obtaining measurements without support interference are even greater than for zero angle of attack. Consequently, the number of reliable base pressure data is extremely limited. During this study a total of seven sources of data were found; unfortunately, all but two had sting-interference effects. Thus, the present study represents only a preliminary identification of possible influential parameters related to angle-of-attack effects.

Pick[19] launched 10-deg sharp cones into a hypersonic stream at angles of attack up to 75 deg. Through telemetered data and trajectory analysis from motion pictures, he was able to determine the base pressure for three Mach numbers and two unit Reynolds numbers. Boundary layers in the unseparated region of the cone surface were determined to be laminar. Pick's data for $\alpha = 0$, 10, and 20 deg are plotted in Fig. 22 on the same coordinates used in Fig. 7 to correlate the cone base pressure for $\alpha = 0$. Also plotted in each part of Fig. 22 is the correlation developed in the present work for $\alpha = 0$, Eq. (8b). The measured base pressures for $\alpha = 10$ and 20 deg are virtually identical and fall somewhat below his data for zero angle of attack. For angles of attack larger than 20 deg (i.e., twice the cone half angle), Pick found that the base pressure begins to increase. Despite the large differences between Pick's data for $\alpha = 0$ and the correlation developed, it is possible to use this information to estimate the effect of α on P_b.

To achieve a correlation and eliminate discrepancies between Pick's data and the present correlation, the base pressure for $\alpha > 0$ was normalized by the corresponding value at $\alpha = 0$. Then for each Mach number, the two measured base pressure ratios (at different unit Reynolds numbers) were averaged. Data for $\alpha = 5$ deg were obtained from interpolation of his measured values. From the previous discussions, the effect of approach Mach number can be eliminated by using the Crocco number. Because the proper geometric scaling

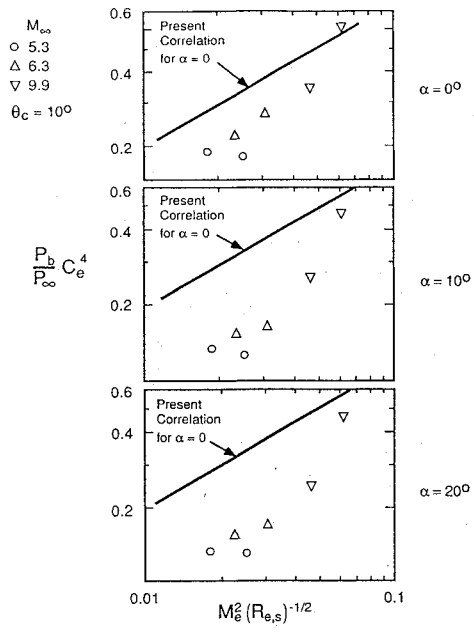

Fig. 22 Effect of angle of attack on base pressure for laminar flow over a blunted 10-deg cone.

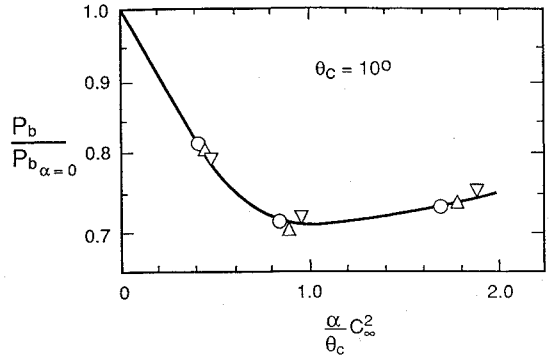

Fig. 23 Correlation of normalized base pressure for a cone at angle of attack.

parameter for the flowfield of cones at angle of attack is the cone half angle, the data are plotted in Fig. 23 using the new correlation parameter $\alpha C_\infty^2/\theta_c$. In practice, we could use the distribution shown in Fig. 23 in conjunction with the laminar base pressure correlation, Eq. (8a), to estimate the cone base pressure for angles of attack up to twice the half angle of the cone. However, the distribution shown in Fig. 23 must be considered a provisional distribution because of the limited data and the discrepancy between the measured base pressures and those discussed earlier.

Additional data are needed to determine if this variation is the same for larger cone angles and turbulent boundary layers. Specific measurements or computations are also needed for the circumferential variation of the Mach number (M_e) before separation, as well as the turning angle of the flow external to the boundary layer. We expect that a circumferentially averaged edge Mach number and pressure, along with an average turning angle, could be used to develop a more general correlation for angle-of-attack influences.

Another study of angle-of-attack effects concerned slender cylindrical bodies. Moore et al.[32] obtained data on a cylinder with a two-caliber tangent ogive nose whose total length-to-diameter ratio (L/D) was 7.2. The experiments were made at approach Mach numbers between 2 and 4.5 and at angles of attack up to 16 deg. The unit Reynolds number for these tests was constant and high enough (2×10^6 ft^{-1}) to ensure a turbulent boundary layer. Data for the zero-angle-of-attack tests on this configuration fell near the correlation line for cylinders given in Fig. 12.

To illustrate the effect of α on this geometry, Fig. 24 plots, using M_∞ as a parameter, the ratio of base pressure for $\alpha \neq 0$ to base pressure for $\alpha = 0$. We see a number of unusual features in the

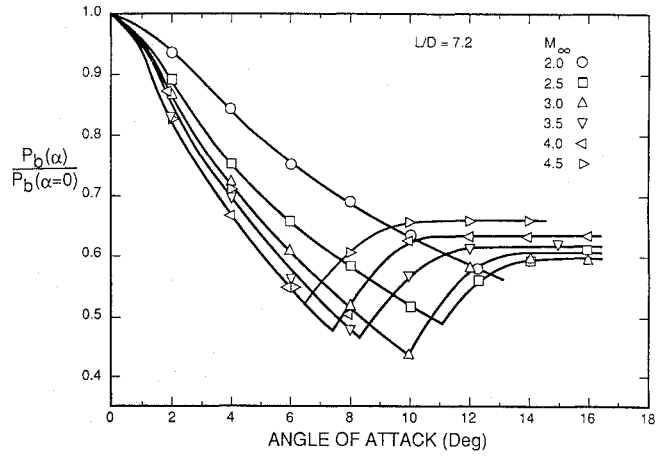

Fig. 24 Normalized base pressure for an ogive-nose cylinder at angle of attack.

trends of this graph. First, similarly to the laminar data for cones, the base pressure initially decreased as the angle of attack increased. The data also showed (except at $M_\infty = 2$) that the base pressure reached a minimum value and then began to increase sharply. If the angle of attack had been increased for $M_\infty = 2$, we expect that it would also have shown a minimum value and then a sharp increase. At large angles of attack, an almost constant value of base pressure was attained. This constant value of P_b appeared to be less sensitive to approach Mach number than the corresponding variations in the low-α regime.

A possible explanation for these trends, which accounts for this dual regime of base pressure (Fig. 24), is as follows. At low angles of attack, a region of moderate crossflow separation exists because of symmetric body vortices on the leeward side of the cylinder. The strength of the body vortex wake increases as the angle of attack increases and as the L/D of the body increases.[49] At the aft end of the body this leeside vortex wake interacts with the recirculation zone associated with the base. For the large-angle-of-attack (or large-L/D) regime, the body vortex wake becomes increasingly stronger and elongated in the direction normal to the cylinder axis. We postulate that the interaction of the body vortex wake and the recirculating base flow fundamentally changes character for very strong, elongated body vortices. This dissimilar interaction could explain the reversal of the base pressure trends illustrated in Fig. 24.

For this investigation, we considered a correlation only for the low-angle-of-attack regime, that is, before the base pressure began a sharp rise with angle of attack. As shown in Fig. 24, the curves for all Mach numbers were essentially linear with angle of attack, and were shifted lower in direct relation to M_∞. Recalling that the laminar data of Pick[19] could be correlated by a parameter proportional to αC_∞^2 (Fig. 23), we considered αC_∞^n for correlating these turbulent data and found that αC_∞^3 produced satisfactory results. The parameter that was neglected in this function was the length-to-diameter ratio of the body. Experimental data of Oberkampf and Bartel[49] showed that the body-vortex strength was approximately quadratic with angle of attack and linear with L/D. Because base pressure is linearly related to angle of attack, this suggests that the base pressure should be proportional to $(L/D)^{\frac{1}{2}}$. Figure 25 shows the correlation of $P_b(\alpha \neq 0)/P_b(\alpha = 0)$ with $\alpha(L/D)^{\frac{1}{2}} C_\infty^3$. Additional data for other L/D values are needed to validate the use of such a correlation. Also note that the angle of attack at which the minimum value of the base pressure occurs also depends on L/D. For example, bodies with an L/D higher than 7.2 will have an angle of attack that is lower than that shown in Fig. 24, after which the base pressure will begin a sharp rise.

Effects of the Ratio of Specific Heat

If we wanted to determine trajectories of vehicles in various planetary atmospheres or in geometries with combustion gases approaching the base region, we could extend the current correlations to gases other than air. Such an extension is not simple; however, the generalized design of the present correlations would allow one to construct

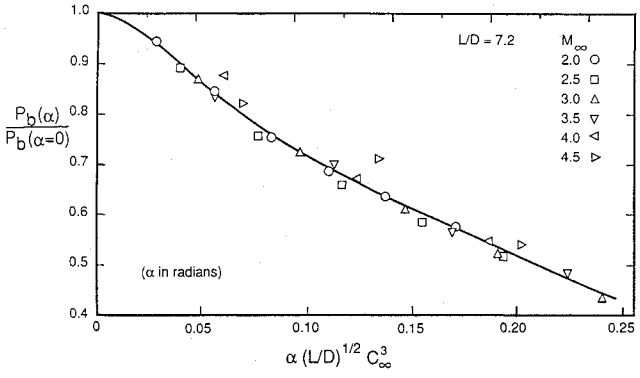

Fig. 25 Correlation of normalized base pressure for an ogive-nose cylinder at angle of attack.

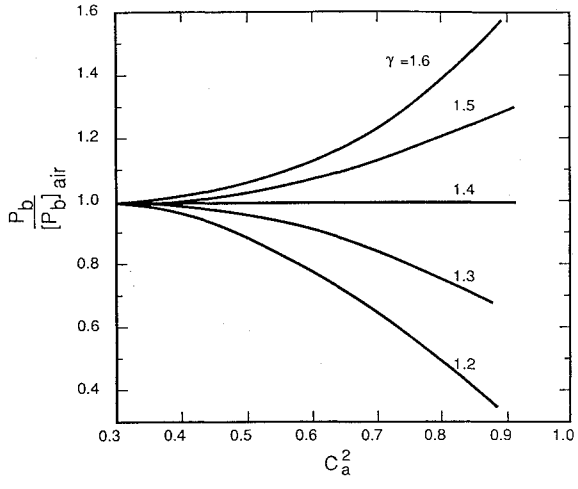

Fig. 26 Effect of specific-heat ratio on normalized base pressure.

new correlations that differ from the present results only in the values of empirical multipliers and exponents.

A first-order estimate of the effect of gas properties on base pressure for planar or cylindrical geometries in the turbulent regime can be obtained by using the classic theory of Korst,[44] which assumes a uniform supersonic flow approaching the shoulder. This flow passes through a Prandtl-Meyer expansion and develops a free shear layer, within which is a stagnating streamline determined from continuity requirements. The external inviscid flow passes through an oblique shock (or Prandtl-Meyer compression) at the recompression region, i.e., wake neck. The correct base pressure occurs when the static pressure downstream of the oblique shock is equal to the stagnation pressure produced by the Mach number of the stagnating streamline (Fig. 4). Thus, the only gas property required for this first-order theory is the ratio of specific heats, γ. The entire computation can be automated easily, and a parametric variation of the ratio P_b/P_1 can be obtained for various values of the approaching Crocco number, C_1 or C_a, upstream of the base.

The effect of γ is shown in Fig. 26, which displays the variation of $P_{b\,\text{gas}}/P_{b\,\text{air}}$ vs C_a^2. A comparison of flows with the same value of M_1 shows a similar distribution. Besides combustion products ($\gamma \approx 1.2$), the range of γ values in this plot encompasses gases such as carbon dioxide, methane ($\gamma \approx 1.2$ to 1.3), and helium ($\gamma = 1.67$). Of course, air, nitrogen, and hydrogen have $\gamma \approx 1.3$ to 1.4, depending on the temperature. It is seen that, for a given approach flow, as γ increases above the value for air, the base pressure also increases. Similarly, as γ decreases below 1.4, the base pressure also decreases. The change in base pressure at constant C_a, or C_1, is also nearly symmetrical with respect to increasing or decreasing γ. That is, $|\Delta P_b|$ is proportional to $|\Delta\gamma|$ for a constant Crocco number.

Figure 26 also shows that the influence of γ becomes large at higher Mach numbers. The actual effect of γ on base drag, however, at hypersonic conditions should be small, because the base pressure is very low at these conditions.

Estimation of Edge Conditions

Laminar and turbulent base pressure correlations for cones depend on the values of the Mach number (or Crocco number) and/or Reynolds number (as well as the static pressure) at the edge of the boundary layer before separation. These edge parameters are important because they characterize the inviscid flow that expands around the shoulder. Satisfactory estimates of these parameters can normally be obtained from numerical solutions to the inviscid flow equations if the proper location is taken in the shock layer. For a sharp cone, the inviscid solutions display nearly constant values of pressure, velocity, and Mach number between the cone surface and the bow shock. However, for blunted cones the shock layer contains a region of rotational flow because of the curved portion of the bow shock wave. The rotationality of the flow is manifested as an entropy gradient in the shock layer. Thus, we observe surface normal gradients of velocity, pressure, temperature, and Mach number outside the boundary layer. In actual viscous flows this entropy gradient in the shock layer tends to flow into (i.e., be swallowed by) the boundary layer as the axial distance along the cone increases. This can be seen graphically in CFD Navier-Stokes solutions by tracing streamlines from the curved portion of the bow shock along the body through the shock layer.

Figure 27 illustrates a typical inviscid solution for a 9-deg cone with 29% blunting at Mach numbers of 4 and 9. This geometry and flow condition are taken from Zarin's[28] experiment. The plot shows profile shapes for total velocity, Mach number, and static pressure between the cone surface and the bow shock at $s/r_n = 30.4$. The thickness of the entropy layer can be approximated by noting the point at which the velocity gradient near the wall disappears. The edge conditions from inviscid flow solutions should be taken at the edge of the entropy layer, indicated as location e in Fig. 27. Results such as these suggest that data from a viscous solution are often not essential for estimating base pressure and heat transfer using the present correlations. However, there are limits to simply using inviscid solutions; they become increasingly less reliable as the entropy layer becomes a larger percentage of the shock-layer thickness. For example, this occurs on a short vehicle ($s/r_n < 10$), particularly as the cone angle decreases.

An example of how a viscous flow solution differs from an inviscid solution is illustrated in Fig. 28. This geometry and flow con-

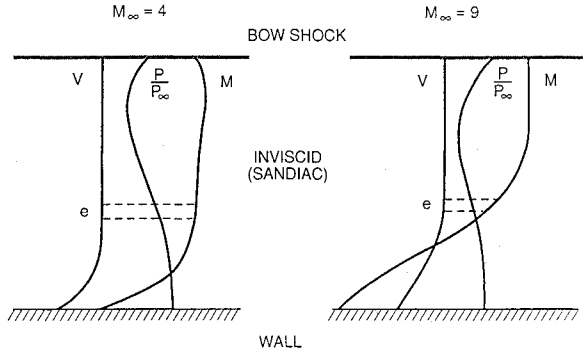

Fig. 27 Computed inviscid flow parameters across the shock layer for $\theta_c = 9$ deg, $r_n/r_b = 0.29$, and $s/r_n = 30.4$.

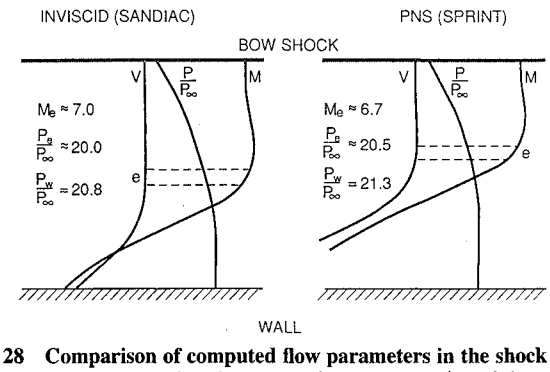

Fig. 28 Comparison of computed flow parameters in the shock layer for inviscid and viscous flow ($M_\infty = 14$, $\theta_c = 15$ deg, $r_n/r_b = 0.2$ and $s/r_n = 15.7$).

dition are from one of Lockman's[10] experiments. The figure shows profiles computed by an Euler code (SANDIAC) and a parabolized Navier-Stokes code (SPRINT). For this geometry, flow conditions, and s/r_n value, the entropy layer is swallowed (i.e., diffused) within the boundary layer. The computed values of the edge Mach number and pressure, as well as the wall pressure, are essentially the same for both cases. For this case the percentage differences between Euler and PNS solutions near the edge of the entropy layer are as follows: Mach number, inviscid is 5% higher; P_e/P_∞, inviscid is 3% lower; and P_w/P_∞, inviscid is 3% lower. Errors of this magnitude are generally less than those associated with either the original experimental data or the correlations developed in this work.

Conclusions

A comprehensive review of experimental data on the base pressure and base heating related to supersonic and hypersonic flight has been completed. We paid particular attention to flight data as well as to wind-tunnel data for models without rear sting support. Using theoretically based correlation parameters, we developed a series of internally consistent, empirical prediction equations for both planar and axisymmetric geometries. These equations are applicable over a wide range of Reynolds and Mach number for laminar and turbulent boundary layers. A wide range of cone and wedge angles and nose bluntness was also included in the data base and correlations.

A feature of this study has been the use of the Crocco number which, unlike the Mach number, is linearly related to velocity. Also unlike the Mach number, the Crocco number has a maximum value of unity. This parameter permits the hypersonic regime to be treated in a more reasonably scaled manner than in past correlations. Improved and wider ranging correlations are obtained by using hypothetical axial-flow downstream conditions. It is also shown that base-plane heat transfer is related to base pressure by a simple power-law and is therefore correlated with the same parameters.

A study of the effect of angle of attack on base pressure for cones and cylinders was also included in this investigation. A new, nondimensional angle-of-attack parameter appears to be capable of correlating the base pressure with its value at $\alpha = 0$. Also included in this analysis is an approximate result for gases with a ratio of specific heats different than air. This correlation would be useful for estimating the drag of vehicles entering different planetary atmospheres or the drag of objects in combustion gases.

The results of the present study should permit the estimation of base pressure and base heating levels with considerably more confidence and over a wider range of conditions than in the past. For example, in addition to the specific geometries examined, the present results would apply to multiconic configurations if the maximum θ_c were less than 20 deg. Also, according to the data reviewed, average base pressures for cones with a small amount of slicing on one side could fall within the general scatter of test data used in developing these correlations. On the other hand, a bent-cone body would likely produce sufficiently asymmetric flow approaching the base so that the present correlations would have to be used with considerable caution.

Acknowledgment

The authors thank Mary McWherter Walker of the Computational Fluid Dynamics Department at Sandia National Laboratories for computing the inviscid and parabolized Navier-Stokes solutions used in this study. The authors also thank David Kuntz and Vincent Amatucci of the Thermophysics Department at Sandia for reviewing this report and making a number of valuable suggestions.

Part of this work was performed at Sandia National Laboratories, which is operated by Martin-Marietta Corp. for the U.S. Department of Energy under Contract DE-AC04-94 AL 8500.

References

[1]Stivers, L. S., "Calculated Pressure Distributions and Components of Total Drag Coefficients for 18 Constant-Volume, Slender Bodies of Revolution at Zero Incidence for Mach Numbers from 2.0 to 12.0, with Experimental Aerodynamic Characteristics for Three of the Bodies," NASA TN D-6536, 1971.

[2]Murthy, S. N. B., and Osborn, J. R., "Base Flow Phenomena With and Without Injection: Experimental Results, Theories, and Bibliography," *Aerodynamics of Base Combustion*, edited by S. N. B. Murthy, Vol. 40, Progress in Astronautics and Aeronautics, AIAA, MIT Press, 1976, pp. 7–210.

[3]Matthews, R. K., private communication, Air Force Arnold Engineering Development Center, Tullahoma, TN, Oct. 1992.

[4]Martellucci, A., Ranlet, J., Schlesinger, A., and Garberoglio, J., "Experimental Study of Near Wakes," Space and Missile Systems Organization, U.S. Air Force, BSD-TR-67-229, Vol. 1, Nov. 1967.

[5]Chapman, D. R., Kuehn, D. M., and Larson, H. K., "Investigation of Separated Flows in Supersonic and Subsonic Flow with Emphasis on the Effect of Transition," NACA TN-3869, 1957.

[6]Chapman, D. R., "An Analysis of Base Pressure at Supersonic Velocities and Comparison with Experiment," NACA Report 1051, 1951.

[7]Kurzweg, H. H., "Interrelationship between Boundary Layer and Base Pressure," *Journal of Aeronautical Sciences*, Vol. 18, No. 11, 1951, pp. 743–748.

[8]Kavanau, L. L., "Base Pressure Studies in Rarefied Supersonic Flows," *Journal of Aeronautical Sciences*, Vol. 23, No. 3, 1956, pp. 193–207.

[9]Lehnert, R., and Schermerhorn, V. L., "Correlation of Base Pressure and Wake Structure of Sharp and Blunt-Nose Cones with Reynolds Number Based on Boundary Layer Momentum Thickness," *Journal of Aero/Space Sciences*, Vol. 26, No. 3, 1959, pp. 185–186.

[10]Lockman, W. K., "Free-Flight Base Pressure and Heating Measurements on Sharp and Blunt Cones in a Shock Tunnel," *AIAA Journal*, Vol. 5, No. 10, 1967, pp. 1898–1900.

[11]Murman, E. M., "Experimental Studies of a Laminar Hypersonic Cone Wake," *AIAA Journal*, Vol. 7, No. 9, 1969, pp. 1724–1730.

[12]Bulmer, B. M., "Study of Base Pressure in Laminar Hypersonic Flow: Re-Entry Flight Measurements," *AIAA Journal*, Vol. 13, No. 10, 1975, pp. 1340–1348.

[13]Reeves, B. L., and Buss, H., "The Near Wake of Axisymmetric Bodies in Hypersonic Flow," *Propulsion and Re-Entry*, Proceedings of the XVIII International Astronautical Conference, Belgrade, Yugoslovia, Sept. 1967, Vol. 3, edited by M. Lunc et al., 1968, pp. 213–219.

[14]Kawecki, E. J., "Comparison of Several Re-Entry Vehicle Base Pressure Correlations," *Journal of Spacecraft and Rockets*, Vol. 14, No. 5, 1977, pp. 284–289.

[15]Starr, R. F., "Base Pressure on Sharp and Blunt Conical Bodies at Supersonic Speeds," *AIAA Journal*, Vol. 15, No. 5, 1977, pp. 753–755.

[16]Dorrance, W. H., *Viscous Hypersonic Flow*, McGraw-Hill, New York, 1962.

[17]White, F. M., *Viscous Fluid Flow*, McGraw-Hill, New York, 1974.

[18]Cassanto, J. M., "Base Pressure Results at $M = 4$ Using Free-Flight and Sting-Supported Models," *AIAA Journal*, Vol. 6, No. 7, 1968, pp. 1411–1414.

[19]Pick, G. S., "Base Pressure Distributions on a Cone at Hypersonic Speeds," *AIAA Journal*, Vol. 10, No. 12, 1972, pp. 1685, 1686.

[20]Badrinarayanan, M. A., "An Experimental Investigation of Base Flows at Supersonic Speeds," *Journal of the Royal Aeronautical Society*, Vol. 65, No. 607, July 1961, pp. 475–482.

[21]Reller, J. O., and Hamaker, F. M., "An Experimental Investigation of the Base Pressure Characteristics of Nonlifting Bodies of Revolution at Mach Numbers form 2.73 to 4.98," NACA TN 3393, March 1955.

[22]Batt, R. G., and Kubota, T., "Experimental Investigation of Laminar Near Wakes behind 20° Wedges at $M_\infty = 6$," *AIAA Journal*, Vol. 6, No. 11, 1968, pp. 2077–2083.

[23]Dewey, C. F., "Near Wake of a Blunt Body at Hypersonic Speeds," *AIAA Journal*, Vol. 3, No. 6, 1965, pp. 1001–1010.

[24]Bulmer, B. M., "Flight-Test Base Pressure Measurements in Turbulent Flow," *AIAA Journal*, Vol. 14, No. 12, 1976, pp. 1783–1785; Sandia National Labs., Report SAND 76-0267, June 1976.

[25]Mark, A., "Free Flight Base Pressure Measurements on 8° Cones," AIAA Paper 78-1347, 1978.

[26]Tanner, M., "Base Pressure Measurements on a Cone at Mach Numbers from $M_\infty = 5$ to 7," *Experiments in Fluids*, Vol. 12, No. 1/2, 1991, pp. 113–118.

[27]Uselton, B. L., and Cyran, F. B., "Sting Interference Effects as Determined by Measurements of Dynamic Stability Derivatives, Surface Pressure, and Base Pressure for Mach Numbers 2 through 8," Arnold Engineering Development Center, TR 79-89, Oct. 1980.

[28]Zarin, N. A., "Base Pressure Measurements on Sharp and Blunt 9° Cones at Mach Numbers from 3.5 to 9.2," *AIAA Journal*, Vol. 4, No. 4, 1966, pp. 743–745.

[29]Pepper, W. B., and Holland, T. R., "Transonic Pressure Measurements on Blunt Cones," Sandia Corp., Report SC-4157 (TR), May 1958.

[30]Wehrend, W. R., "An Experimental Evaluation of Aerodynamic Damping Moments of Cones with Different Centers of Rotation," NASA TN D-1768, March 1963.

[31]Kayser, L. D., "Base Pressure Measurements on a Projectile Shape at Mach Numbers from 0.91 to 1.20," Ballistic Research Lab., Memorandum Report ARBRL-MR-03353, April 1984.

[32]Moore, F. G., Hymer, T., and Wilcox, F. J., "Improved Empirical Model for Base Drag Prediction on Missile Configurations Based on New Wind Tunnel Data," Naval Surface Warfare Center, Report NSWCDD/TR-92/509, Oct. 1992.
[33]Seiling, W. R., and Page, R. H., "A Re-Examination of Sting Interference Effects," AIAA Paper 70-585, May 1970.
[34]Goecke, S. A., "Comparison of Wind-Tunnel and Flight-Measured Base Pressures from the Sharp-Leading-Edge Upper Vertical Fin of the X-15 Airplane for Turbulent Flow at Mach Numbers from 1.5 to 5.0," NASA TN D-6348, May 1971.
[35]McDonald, H., "The Turbulent Base Pressure Problem: a Comparison between a Theory and Some Experimental Evidence," British Aircraft Corp., Report Ae 194, April 1965.
[36]Noack, R. W., and Lopez, A. R., "Inviscid Flow Field Analysis of Complex Reentry Vehicles: Volume 1, Description of Numerical Methods," Sandia National Labs., Rep. SAND87-0776/1, Oct. 1988.
[37]McWherter, M., Noack, R. W., and Oberkampf, W. L., "Evaluation of Boundary-Layer and Parabolized Navier-Stokes Solutions for Re-Entry Vehicles," *Journal of Spacecraft and Rockets*, Vol. 23, No. 1, 1986, pp. 70–78.
[38]Daywitt, J. E., Brant, D., and Bosworth, F., "Computational Technique for Three-Dimensional Inviscid Flowfields about Reentry Vehicles," Space and Missile Systems Organization, TR-79-5, April 1978.
[39]Reeves, B. L., and Lees, L., "Theory of Laminar Near Wake of Blunt Bodies in Hypersonic Flow," *AIAA Journal*, Vol. 3, No. 11, 1965, pp. 2061–2074.
[40]Stalnaker, J. F., Nicholson, L. A., Hanline, D. S., and McGraw, E. H., "Improvements to the AFWAL Parabolized Navier-Stokes Code Formulation," Air Force Wright Aeronautical Labs. AFWAL-TR-86-3076, Sept. 1986.
[41]Walker, M. M., and McBride, D. D., "Comparisons of CFD Flow Field Solutions with Experimental Data at Mach 14," AIAA Paper 86-0742-CP, March 1986.
[42]Oberkampf, W. L., Aeschliman, D. P., and Walker, M. M., "Joint Computational/Experimental Aerodynamics Research on a Hypersonic Vehicle," AGARD Conference on Theoretical and Experimental Methods in Hypersonic Flows, Paper No. 23, Torino, Italy, May 1992.
[43]Chapman, D. R., "A Theoretical Analysis of Heat Transfer in Regions of Separated Flow," NACA TN-3792, 1956.
[44]Korst, H. H., "A Theory for Base Pressures in Transonic and Supersonic Flow," *Journal of Applied Mechanics, Transactions of the American Society of Mechanical Engineers*, Vol. 23, 1956, pp. 593–600.
[45]McAlister, K. W., Stewart, D. A., and Peterson, V. L., "Aerodynamic Characteristics of a Large-Angle Blunt Cone With and Without Fence-Type Afterbodies," NASA TN D-6269, April 1971.
[46]Bulmer, B. M., "Re-Entry Vehicle Base Pressure and Heat Transfer Measurements at $M_\infty = 18$," *AIAA Journal*, Vol. 13, No. 4, 1975, pp. 522–524.
[47]Bulmer, B. M., "Heat Transfer Measurements in a Separated Laminar Base Flow," *Journal of Spacecraft and Rockets*, Vol. 14, No. 11, 1977, pp. 701, 702.
[48]Muntz, E. P., and Softly, E. J., "A Study of Laminar Near Wakes," *AIAA Journal*, Vol. 4, No. 6, 1966, pp. 961–968.
[49]Oberkampf, W. L., and Bartel, T. J., "Symmetric Body Vortex Wake Characteristics in Supersonic Flow," *AIAA Journal*, Vol. 18, No. 11, 1980, pp. 1289–1297.